Università degli Studi del Sannio

Facoltà di ingegneria

Corso di Laurea Magistrale in Ingegneria Energetica

Master Thesis

in

Fisica Generale

Simulation and experimental studies on electron cloud effects in particle accelerators

Thesis Advisor:

Prof. Stefania Petracca

CERN Co-Advisors:

Dott. Roberto Cimino

Ing. Giovanni Iadarola

Ing. Giovanni Rumolo

Author:

Annalisa Romano

matr. 389000023

Academic Year 2013-2014

" If your dreams do not scare you,
they are not big enough "

Ellen Johnson Sirleaf

"A mia nonna,
cosí lontane eppure cosí vicine"

Abstract

Electron Cloud (EC) effects represent a serious limitation for particle accelerators operating with intense beams of positively charged particles. This Master thesis work presents simulation and experimental studies on EC effects carried out in collaboration with the European Organization for Nuclear Research (CERN) in Geneva and with the INFN-LNF laboratories in Frascati. During the Long Shutdown 1 (LS1, 2013-2014), a new detector for EC measurements has been installed in one of the main magnets of the CERN Proton Synchrotron (PS) to study the EC formation in presence of a strong magnetic field. The aim is to develop a reliable EC model of the PS vacuum chamber in order to identify possible limitation for the future high intensity and high brightness beams foreseen by Large Hadron Collider (LHC) Injectors Upgrade (LIU) project. Numerical simulations with the new PyECLOUD code were performed in order to quantify the expected signal at the detector under different beam conditions. The experimental activity, carried out at the INFN-LNF, was focused on the characterization of Cu foams as a mean for mitigating EC effects.

Contents

List of Figures

Abbreviations

bl	**b**unch **l**ength
CDF	**C**omulative **D**istribution **F**unction
CERN	**European Organization for Nuclear Research**
EC	**E**lectron **C**loud
HL-LHC	**H**igh **L**uminosity - **LHC**
L	**L**uminosity
LHC	**L**arge **H**adron **C**ollider
MD	**M**achine **D**evelopment
MU	**M**agnet **U**nits
MP	**M**acro**P**article
PY	**P**hoton **Y**ield
ppb	**p**rotons **p**er **b**unch
PS	**P**roton **S**ynchroton
PSB	**P**roton **S**ynchroton **B**oosters
RF	**R**adio **F**requency
SC	**S**uper **C**onducting
SEY	**S**econdary **E**lectron **Y**ield
SR	**S**ynchroton **R**adiation
SPS	**S**uper **P**roton **S**ynchroton

Introduction

The Electron Cloud (EC) is a detrimental effect that can occur in accelerators which operate with positively charged particles. In the beam chambers, free low energy electrons can be generated by different mechanism like ionization of the residual gas or the photoemission of the beam chamber's walls due to the synchrotron radiation emitted by the beam. These electrons, interacting with the circulating beam, can be accelerated before impacting against the chamber's wall. According to the their impact energy and to the Secondary Electron Yield (SEY) of the surface, secondary electrons can be generated. This mechanism can drive an avalanche electron multiplication with the formation of a so called EC in the chamber.

To achieve high energies and high brightness considered key performance quantities of a particle collider, very high quality particle beams are wanted. In particular, high intensity and low transverse emittances are required properties. The presence of a large electron density in the chamber as well as a strong electron flux on the chamber's walls can limit the achievable performance of the accelerator since it introduces transverse instabilities, transverse emittance growth, particle losses, vacuum degradation and heating of the chamber's surface. For these reasons, important efforts are devoted to improve the modeling and understanding of this phenomenon and to define suitable mitigation techniques.

In this work the EC formation is addressed through both simulation and experimental activities performed in collaboration with the European Organization for Nuclear Research (CERN) and with the Laboratorio di Frascati of the Istituto Nazionale di Fisica Nucleare (INFN-LNF).

CERN has a long experience in EC build up simulation, mostly carried out with the ECLOUD code, developed and maintained at CERN since 1997. Recently, a new and fully reorganized code has been developed to study the EC effects in the Large Hadron Collider (LHC) and in its injectors, the Proton Synchrotron (PS) and the Super Proton Synchrotron (SPS). This code is named PyECLOUD since it is written in Python and inherits the physics model of ECLOUD code.

In the present thesis work, PyECLOUD simulations have been employed to study the EC build up in the CERN PS. The PS is a key component in the CERN accelerator complex since its main task is to produce the LHC nominal beam type used for physics by the LHC experiments. EC effects have been observed at the PS during the last stages of the cycle of the production of the LHC type beams. Although presently these beams are not degraded by the interaction with the EC, which develops only during few milliseconds before extraction, the question if this effect could degrade the future high intensity and high brightness beams foreseen by the LHC Injectors Upgrade (LIU) project is still open. Therefore several studies are being carried out employing both simulations and experimental measurements. The aim is to develop a reliable EC model of the PS vacuum chambers in order to identify possible future limitations and find suitable countermeasures.

In this framework a new detector for EC measurements has been installed in one of the main magnets of the machine to study the EC formation in presence of a strong magnetic field. The EC detector is a shielded pickup able to measure the electron flux to the chamber's wall.

To complement this experimental activity, numerical simulations with the PyECLOUD code were required in order to quantify the expected signal at the detector under different beam conditions. The presence of the strong and non-uniform magnetic field of the PS combined function magnet makes these simulations quite challenging from the numerical point of view. This has required several preliminary checks to validate the modeling of EC detectors in PyECLOUD and to identify a correct simulation setup, allowing to achieve a good balance between simulation accuracy and computation time. Due to design constraints, the detector is slightly displaced with respect to the vertical axis of the chamber cross section. For this reason the dependence of the detected signal on the radial position of the beam also had to be investigated.

The last part of this thesis is dedicated to the experimental work carries out at the INFN-LNF laboratory in Frascati. This activity was mainly devoted to the characterization of Cu foams, available from the market, and their qualification in terms of SEY, vacuum behavior, photo-desorption yield, in order to investigate their capability of suppressing the EC in a vacuum chamber.

The thesis is organized in four chapters. The first chapter introduces some useful fundamental concepts to understand the EC build up mechanism in particle accelerators. The second chapter provides a brief introduction to the CERN PS structure and to the geometry and proprieties of the EC detector. The development of the simulation model for the PS EC detector and the results of our simulation campaign will be discussed in the third chapter. Finally, the experimental studies on Cu foams and their properties are described in the fourth chapter.

Chapter 1

Basic concepts of the Electron Cloud build up

Since 1965, the EC phenomenon has been observed in several storage rings, which operate with intense and positively charged particle beams (e.g positrons, protons, heavy ions), like the Relativistic Heavy Ion Collider (RHIC) in the USA [2], the KEKB electron positron collider in Japan [3], the DAΦNE electron positron collider in Italy [4] and, more recently, the CERN LHC[5]. Once an EC is formed, it interacts with beam inducing many detrimental effects on the machine performances, especially for high-intesity ones, such as: voltage breakdown in RF devices, pressure rise , surface heating [6–8], beam instability.

A qualitative picture of the EC buildup at a section of an accelerator operated with bunches of positively charged particles is sketched in Fig. 1.1 (see also [9]).

During a bunch passage, electrons can be generated by ionization of the residual gas in the beam chamber and photoemission from the chamber's wall due to the synchrotron radiation emitted by the beam; they are called *primary* or *seed electrons*. These primary electrons are usually insufficient to lead to a significant EC density. However, if the seeds see the passing particle bunch, they are attracted due to the Coulomb force and gain energy (up to several hundreds of eV). Due to

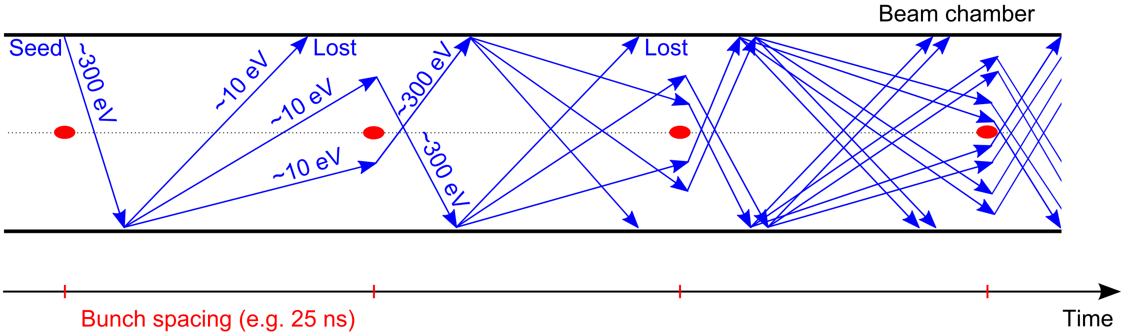

FIGURE 1.1: Schematic of the formation of an electron cloud in a particle accelerator (a similar sketch can be found in [9]).

this acceleration, the electrons impact against the accelerator walls, thus producing a cascade of low energy electrons: *secondary electrons*. Such secondaries have energies up to few tens of eV and, if they impact the wall with these energies, they are absorbed or elastically reflected but cannot produce any secondary electrons. On the other hand, if they survive until the passage of the following bunch they can in turn be accelerated, impinging the walls and produce other secondaries. The number of secondary electrons that can be generated is strongly dependent on the beam pipe geometry, beam structure (bunch spacing, bunch length, intensity, radial position) and on properties of the chamber's surface. Under certain conditions, the number of electrons in the chamber can grow exponentially in time and, consequently, also the cloud density. This avalanche electron multiplication is called **multipactor effect**.

The present chapter will describe the origin and the basic features of the EC buildup mechanism, how it can affect the performances of particle accelerators and which are the possible mitigation strategies.

1.1 Primary electron production

According to the type of machine and the energy of the accelerated particles, the EC buildup is related to two different mechanism for the generation of primary electrons: the beam induced an ionization of the residual gas and the photoemission due to synchrotron radiation.

- **Residual gas ionization:** the particle of the beam can ionize the molecules of the residual gas in the beam chambers (where vacuum pressures are typically below 10^{-8} mbar) producing free electrons. The local electron production rate per unit volume in the beam chamber is given by:

$$\frac{dn_{\text{ion}}}{dt} = \sigma_{\text{ion}} n_{\text{gas}} \phi_p \tag{1.1}$$

  where σ_{ion} is the ionization cross section of the residual gas [10], n_{gas} is the residual gas density (supposed to be uniform in space and constant on the time scale of few beam revolutions), and ϕ_p is the beam particle flux (per unit area)[11]. For proton beams, the number of seeds produced by gas ionization is higher for beam energies below 2 TeV[12]. For this reason, the EC effects has been observed to occur also in the PS and the SPS where the energy goes up to 26 GeV for the PS and up to 450 GeV for the SPS.

- **Photoemission due to synchrotron radiation:** synchrotron radiation is the emission of photons that occurs when a particle beam undergoes a transverse acceleration [13, 14], for example in a bending magnet. The total power emitted by the beam due to the bending dipoles can be written as:

$$P = \frac{q\gamma_{\text{rel}}^4}{3\varepsilon_0 \rho} I_{\text{beam}} \tag{1.2}$$

  where q is the particle charge, γ_{rel} is the relativistic factor, I_{beam} is the beam current.

  The minimum photon energy needed to create a photoelectron depends on the beam chamber's material work function, that typically is of few eV. If the beam energy is large enough, the photons can extract electrons from the chamber's wall [15]. These electrons are typically called "photoelectrons" and can constitute the main source of primary electrons in the buildup of the EC, when the energy of the beam is large enough, for example in the LHC at collision energy. The synchrotron radiation is emitted in the direction tangent to the beam trajectory. The number of electrons produced per incident photon is defined as the "Photoelectron Yield" of the chamber surface, which depends on several parameters like the photon energy, the angle of incidence and the properties of the technical surface.

1.2 Secondary electron emission

The capability of a solid surface to emit secondary electrons, once it is irradiated by electrons, is called $\delta(E)$. It is a function of the primary electron energy, its angle of incidence and of the composition and history of the chamber surface. The SEY is defined as the ratio between the electron current impinging onto wall and the corresponding emitted current:

$$\delta(E) = \frac{I_{\mathrm{emit}}(E)}{I_{\mathrm{imp}}(E)} \tag{1.3}$$

Typically for materials employed for accelerators vacuum chamber, this function has a maximum value (δ_{max}) in a range of $1 \div 3$ at an energy of $200 \div 600$ eV.

A typical SEY curve is presented in Fig. 1.2, this quantity can in turn be decomposed in two main components following the equation [11]:

$$\delta(E) = \delta_{\mathrm{elas}}(E) + \delta_{\mathrm{true}}(E) \tag{1.4}$$

where $\delta_{\mathrm{elas}}(E)$ and $\delta_{\mathrm{true}}(E)$ correspond respectively to electrons which are elastically reflected by the surface and to the so called "true secondaries". The first component, corresponding to the green curve in Fig. 1.2, can be parametrized as:

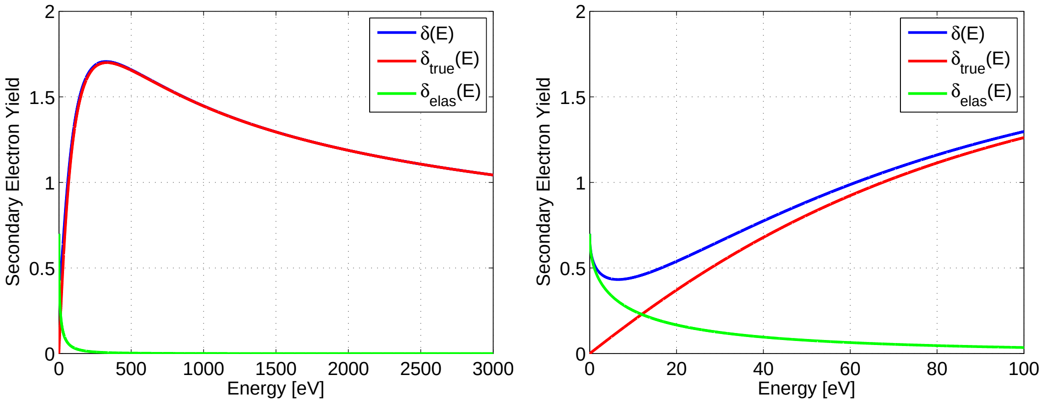

FIGURE 1.2: Left: SEY curve for $\delta_{\max} = 1.7$ - elastic component $\delta_{\text{elas}}(E)$, "true secondary" component $\delta_{\text{true}}(E)$, and total $\delta(E)$. Right: zoom on the low energy region [11].

$$\delta_{\text{elas}}(E) = R_0 \left(\frac{\sqrt{E} - \sqrt{E + E_0}}{\sqrt{E} + \sqrt{E + E_0}} \right)^2 \tag{1.5}$$

where R_0 and E_0 are two free parameters of the model [16]. These electrons are generated by an elastic interaction with the surface of chamber and are emitted with the same energy with which they impacted on the surface. The "true secondary" component has the form:

$$\delta_{\text{true}}(E) = \delta_{\max} \frac{s \dfrac{E}{E_{\max}}}{s - 1 + \left(\dfrac{E}{E_{\max}} \right)^s} \tag{1.6}$$

where s is a free parameter and $E_{\max}$ is the value of energy corresponding to the maximum SEY curve. These electrons are emitted from the surface of the chamber after the impact of the electrons, which have enough energy to win the work function of the material. It is quite intuitive to understand that the essential ingredient for the build-up of the EC is the SEY of the chamber surface.

1.3 The Electron Cloud build up mechanism

If we want to find a simple analytical model to describe this process, considering an empty chamber before the injection and a train of uniformly spaced bunches, we can write [11]:

$$n_{i+1} = \delta_{\mathrm{eff},\,i}\, n_i + n_0 \tag{1.7}$$

where n_{i+1} is the number of electrons in the chamber at the instant t_i, right before of the i-th bunch, n_0 the number of seeds generated after the first passage and $\delta_{\mathrm{eff},\,i}\, n_i$ which defines the average of $\delta(E)$ over all electron-wall collision during the time window (such a quantity can also be negative, when the wall acts like a net electron absorber). The quantity $\delta_{\mathrm{eff},\,i}$ can be directly related to the SEY of the chamber's surface $\delta(E)$ and to the energy spectrum of the impacting electrons, since we can write:

$$n_{i+1} = n_i + \int_0^{\infty} \int_{t_i}^{t_{i+1}} \Phi(E,t)\,(\delta(E) - 1)\,dt\,dE + n_0 \tag{1.8}$$

where:

$$\Phi(E,t) = \frac{dn}{dE} \tag{1.9}$$

is the instantaneous energy spectrum of the electrons impinging the wall. If we define the normalized energy spectrum for the the i-th bunch passage as:

$$\phi_i(E) = \frac{1}{n_i} \int_{t_i}^{t_{i+1}} \Phi(E,t)dt \tag{1.10}$$

we can rewrite the Eq. 1.8 as:

$$n_{i+1} = n_i \left(1 + \int_0^{\infty} \phi_i(E)\,(\delta(E) - 1)\,dE\right) + n_0 \tag{1.11}$$

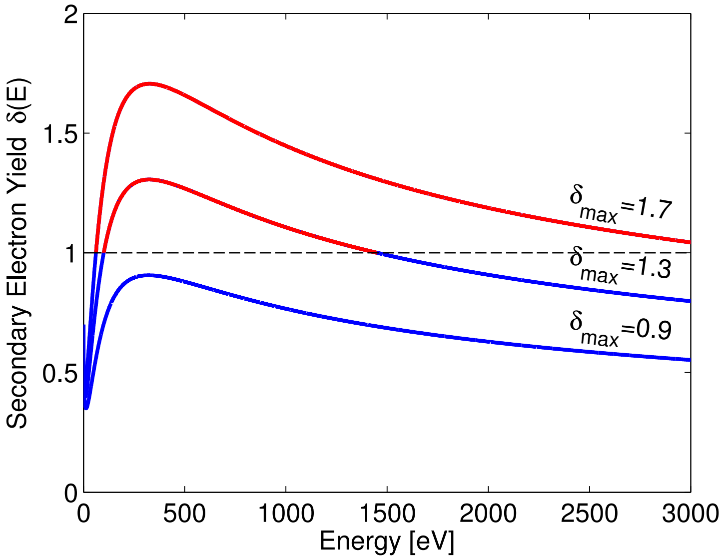

FIGURE 1.3: SEY curve for different values of the $\delta_{\max}$ parameter. The values for which the material behaves as electron absorber or emitter are plotted in blue and red respectively [11].

and, comparing against Eq. 1.7, we obtain:

$$\delta_{\text{eff},\,i} = 1 + \int_0^\infty \phi_i(E)\,(\delta(E) - 1)\,dE \tag{1.12}$$

As shown in Fig. 1.3, for different values of $\delta_{\max}$ it is possible to recognize two regions of the SEY curve depicted in blue and red. The blue one is for $\delta(E) < 1$, which means that the walls act as an electron absorber; in the other case, for $\delta(E) > 1$, the walls act as an electron emitter.

If we suppose that the electrons do not influence each other's trajectory, which means that the Coulomb forces between them are negligible, we can assume that $\delta_{\text{eff},\,i}$ does not depend in the bunch index:

$$\phi_i(E) = \phi(E) \tag{1.13}$$

$$\delta_{\text{eff},\,i} = \delta_{\text{eff}} \tag{1.14}$$

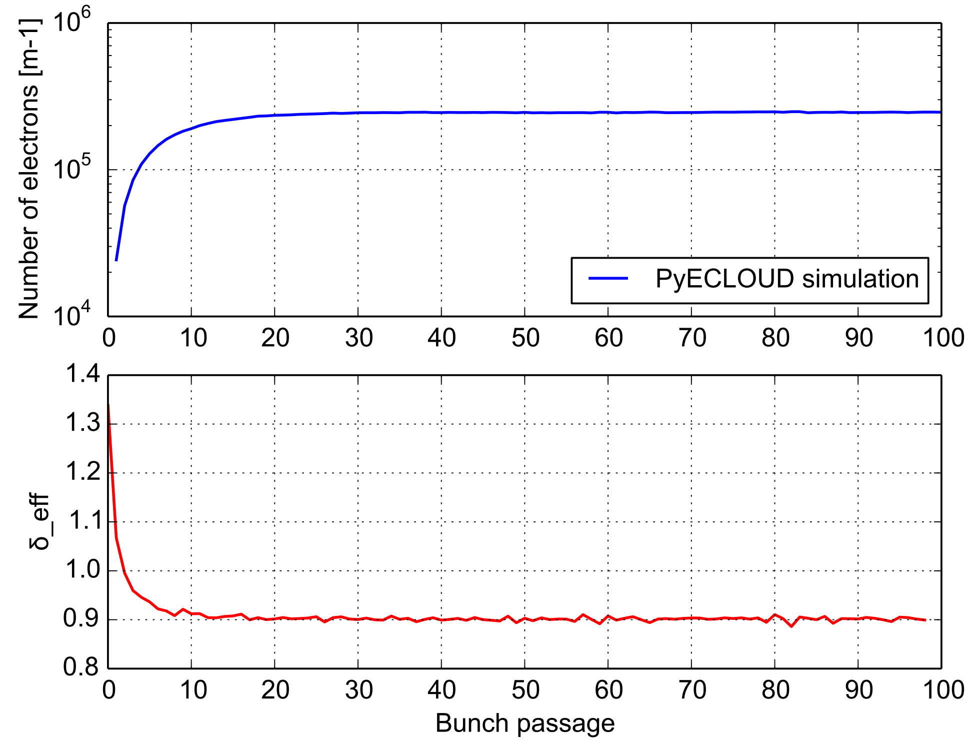

(a) Simulated EC build up for $\delta_{\text{max}} = 1.10$. Top: number of electrons for each bunch passage. Bottom: δ_{eff} computed by Eq. 1.7

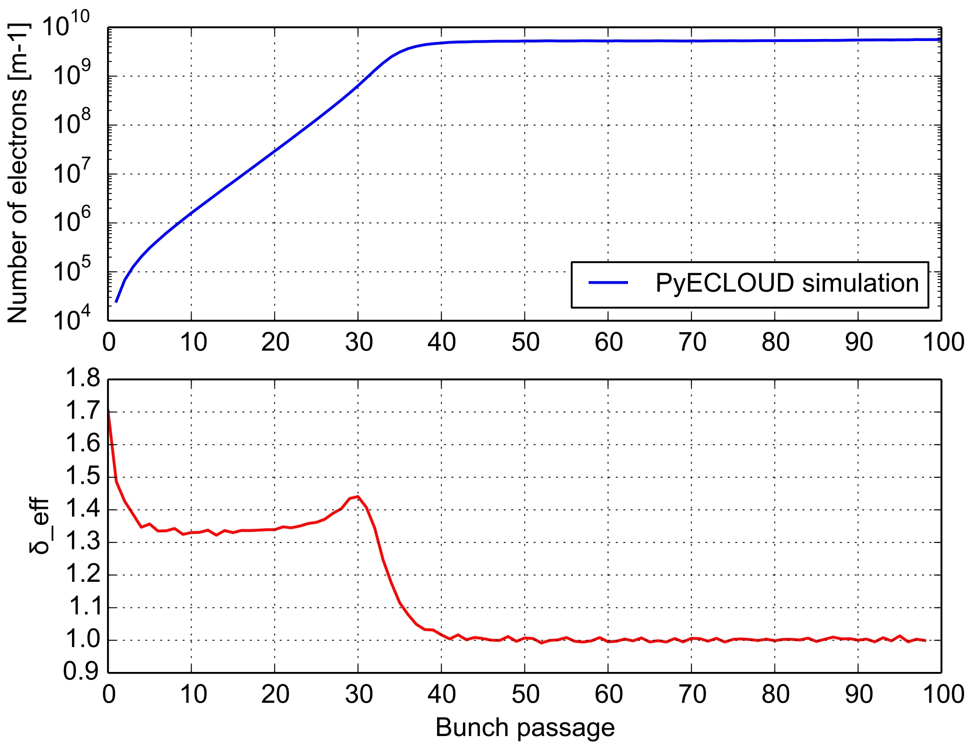

(b) Simulated EC build up for $\delta_{\text{max}} = 1.80$. Top: number of electrons for each bunch passage. Bottom: δ_{eff} computed by Eq. 1.7

FIGURE 1.4: Simulated EC build up for two possible value of δ_{max}

In these conditions by recursively applying Eq. 1.11 we find:

$$n_i = n_0 \sum_{k=1}^{i} \delta_{\text{eff}}^k \tag{1.15}$$

which is a partial sum of a geometric series and can be written as:

$$n_i = n_0 \frac{1 - \delta_{\text{eff}}^i}{1 - \delta_{\text{eff}}} \tag{1.16}$$

According to this, it is possible to define two different conditions (see Eq. 1.12):

- $\delta_{\text{eff}} < 1$: the EC grows linearly in time following beam injection into an empty chamber and, after, it tends to a constant value, which is essentially an equilibrium condition between primary electron production and electron absorption at the chamber's wall. This regime is called as **"seed accumulation regime"** [3, 11].
- $\delta_{\text{eff}} > 1$: the number of electrons in the chamber grows exponentially; this condition is called as **"multipacting regime"** because it indeeds an avalanche multiplication of electrons driven by secondary emission. This build up process stops when the EC space-charge is strong enough to repel the electrons against the walls of the chamber, at which point $\delta_{\text{eff,}}$ becomes equal to 1 and a dynamical equilibrium is reached.

The value of δ_{max} for which $\delta_{\text{eff}} = 1$ is called **"multipacting threshold"** and separates the seed accumulation and the multipacting regimes. It can be easily recognized plotting the number of electrons in the beam chamber versus the SEY.

1.4 Impact of EC effects on the accelerator's performances

The presence of EC in the beam chamber can significantly degrade the performance of particles accelerators through different effects [11]:

- **Transverse beam instabilities**: the presence of the EC on the particle beam can drive transverse instabilities. Both "coupled bunch" instabilities and intra-bunch motion [17] can be observed leading to fast transverse emittance blowup and particle losses, which in many cases can prevent a safe operation of the accelerator. Due to the important high frequency content, the conventional transverse feedback systems are usually ineffective in controlling EC induced instabilities.
- **Incoherent beam effects:** the interaction of the beam with the EC can drive incoherent effects as slow emittance blow up, particle losses, transverse tune spread, which are particularly worrying in storage rings and particle colliders where the aim is to store the beam in the ring for a very long time (several hours) while preserving the beam quality.
- **Vacuum degradation:** the electron flux on the chamber's wall stimulates the desorption of gas molecules from the surface which results in an increased residual gas density in the beam chamber, and therefore in a pressure increase.
- **Heat load:** the electrons also deposit energy on the chamber's wall. This effect is very important because some accelerator devices operate at cryogenic temperature (e.g the superconducting magnets of the LHC) and the heat load can easily reach the cooling capacity limit of their cryogenic system [18].

1.5 Conditioning and Mitigation

As we have seen, accelerator walls surface properties, like SEY, photon reflectivity and photoelectron yield play an important role in governing EC formation. For these reasons, the knowledge of photo yield and X-ray reflectivity is very important for optimizing ultimate performance at accelerators. Generally countermeasures implemented today are of two kind: active or passive [3, 19]. The first one introduces an external electric or magnetic fields in order to reduce the EC formation, for example:

- **Clearing electrodes** can reduce the electron density around the beam by absorbing or repelling electrons through a static electric field. These kind of electrodes were tested in KEKB positron ring and a reasonable reduction of the EC was obtained. Nevertheless the presence of electrodes may induce impedance problems and in most accelerator it is not easy to find the space to accommodate them.
- **Solenoids:** implementing weak solenoidal fields it is possible to trap the electrons close to the chamber walls reducing the multipacting effect.

Passive mechanisms, that have been employed at various machines, aim to the reduction of the surface parameters as SEY and Photoelectron Yield and include:

- **Low SEY Coatings:** coat the vacuum chamber with low-emission substances such as TiN, TiZrV or amorphous carbon. It represents the ideal solution to solve most of the EC problems related to the instabilities. An example of this application is the amorphous carbon thin films that have been applied in the CERN SPS (e.g $\delta_{\max}$ of amorphous carbon close to 1.0). Experimental results have shown a completely suppression of EC for LHC beam type beams in the liners even after 3 months of air venting and no performance deterioration is observed after more than one year of SPS operation [20].

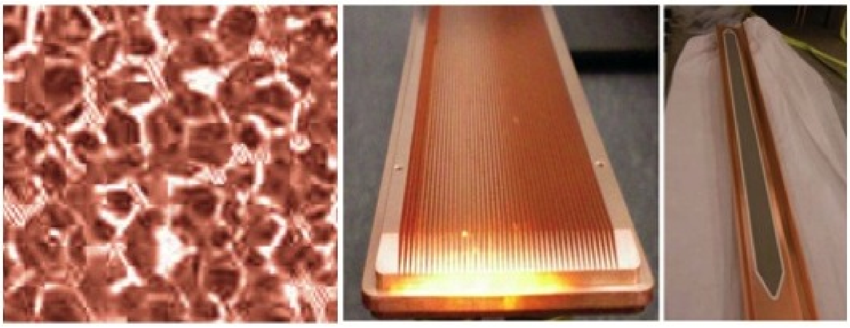

FIGURE 1.5: Several mitigation techniques for the EC. Left: Sponge material. Center: Grooves. Right: Clearing Electrodes

- **Geometrical modification:** this idea is based on the fact that electrons contributing to SEY have an energy distribution peaked at very low kinetic energy. Introducing roughness on the surface of chamber like grooves, rough material coating or sponge, there is the possibility that a fraction of secondaries are trapped and can not escape away from the surface. Several studies have been done in this sense, both at CERN and INFN-LNF. In particular, we will analyze the role of the Cu sponge in the Chap. 4.

- **Surface conditioning:** experimental studies have shown that the EC effects in an accelerator can be self-mitigating when the surface of the vacuum chamber is exposed to prolonged electron irradiation. This modification of the material property is called "Electron Scrubbing". It was observed that an electron bombardment from the EC itself can lower the SEY of the chamber walls and gradually reduce the amount of EC. The reduction of the SEY depends on the electron dose which irradiates the surface [11] and steam from a gradual graphitization of the surface.

1.6 EC simulation code: PyECLOUD

In the past, many of simulations were carried out with the ECLOUD code, developed and maintained at CERN since 1997. Recently, due to its not modular structure and to the programming language, this code has been fully reorganized,

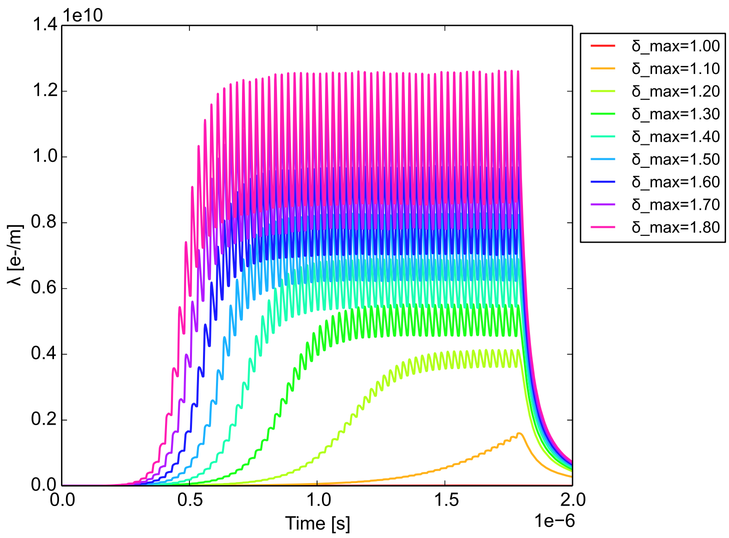

FIGURE 1.6: Simulated EC build up for different value of δ_{max}

several features have been modified obtaining substantial improvements in terms of accuracy, speed and reliability. The new code has been called PyECLOUD since it is written in Python and is largely based on the physical models of the ECLOUD code.

PyECLOUD is a 2D code where the electrons of the cloud are grouped in Macroparticles (MPs) in order to achieve a reasonable computational burden. The beam distribution is assigned *a priori* and it is not affected by Columbian forces from the electrons. With the assumption of ”rigid beam”, it is possible to study the evolution of the EC but not its effects on the beam.

The dynamics of MP system is simulated following the flow diagram sketched in Fig. 1.7 [21]:

- At each time step, a certain number of primary MPs are generated due to residual gas ionization and/or to photoemission (see Sec. 1.1) in a thin slice around a section of the beam pipe.

- The total electric field acting on each MP is computed as sum of the field generated by the beam and the space charge field of the electron cloud itself. The electric field, due to the distributed source, is given by:

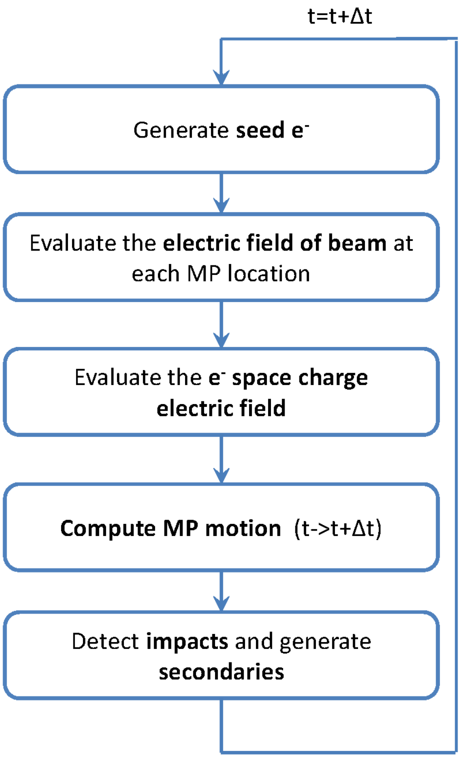

FIGURE 1.7: Flowchart representing PyECLOUD main loop [21]

$$\mathbf{E}(x, y, s, t) = \mathbf{E}_{\perp}(x, y)\lambda(s - ct) \tag{1.17}$$

where $\mathbf{E}_{\perp}(x, y)$ is the transverse electric field, in order to take into account the chamber's profile, it can be evaluated or using the Maxwell's equation or analytically using the Bassetti-Erskine), $\lambda(s - ct)$ is the longitudinal line beam density at the section s at the instant t.

- The space charge contribution is calculated by a classical Particle in Cell (PIC) algorithm, where the finite difference method is employed to solve the Poisson equation with perfectly conducting boundary condition on the beam chamber.

- Once that the total electric field is known, the equations of motion are integrated and the MP positions and momenta are updated accordingly. At this stage the presence of an externally applied magnetic field can also be taken into account.

- At each time step, a certain number of MPs can hit the wall and a secondary emission process is applied to generate emitted electrons.

Since the EC build up can drive an exponential rise of the number of electrons, the MP size is dynamically adapted during the simulation in order to have a computationally affordable number of MPs.

Chapter 2

The CERN Proton Synchrotron

The first particle accelerator was built in the 1920s to investigate the structure of the atomic nucleus. Since then, more and more energetic particle accelerators have been designed to investigate many other aspects of particle physics and to reproduce the conditions that existed within a billion of second after the big bang.

CERN operates the largest particle accelerator ever built. The path of a proton accelerated throughout the accelerator complex at CERN is following the Fig. 2.1: hydrogen atoms are stored in gas form and then protons are obtained by stripping electrons from them. Protons are accelerated up to 50 MeV by a in linear accelerator (LINAC2) into Proton Synchrotron Booster (PSB). The booster accelerates them to 1.4 GeV and transfers the beam into the PS where it is accelerated to 25 GeV. Protons are then sent to the SPS where they increase their energy up to 450 GeV. Finally, they are transferred to the LHC, the world's largest and most powerful particle accelerator. It mainly consists of 27 Km underground ring of superconducting magnets, where two beams of particles are accelerated up to 7 TeV and are collided with high energies for physics experiments. A large part of the work presented in this thesis will focus on EC effects in the CERN PS.

The PS first proton beam was accelerated on 24 November 1959, becoming for a brief period the world's highest energy particle accelerator. Over the years, an increasing number of experiments required the highest possible beam intensity

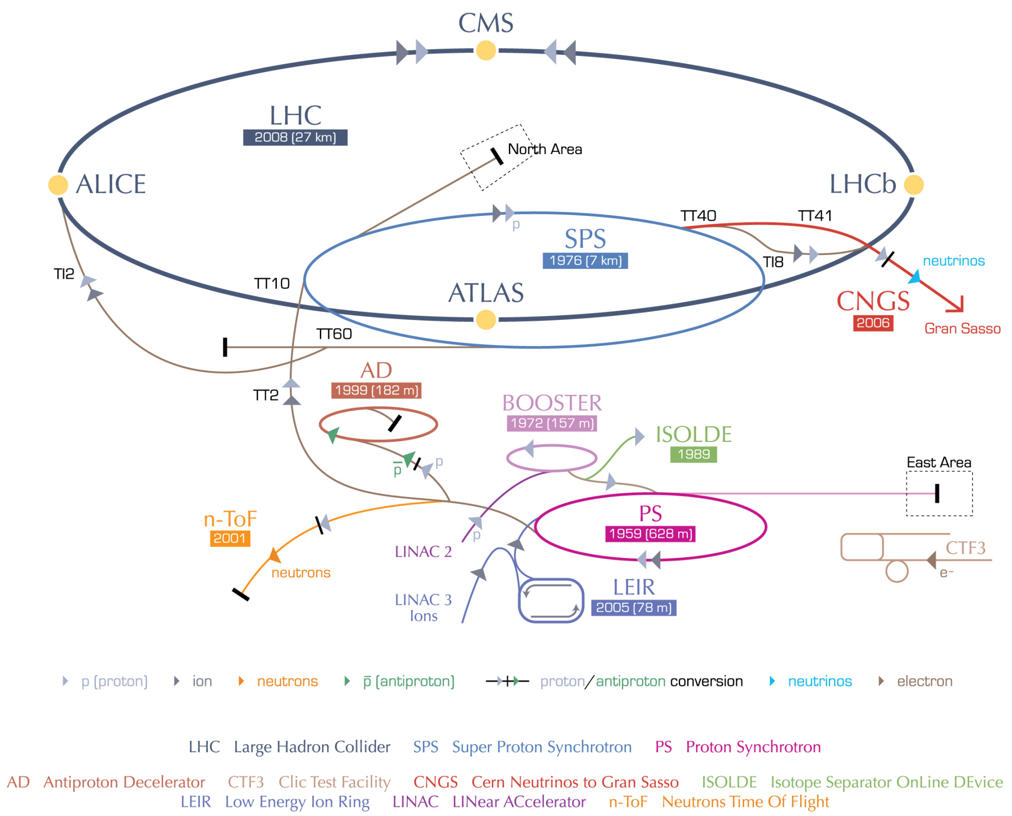

Figure 2.1: CERN accelerator complex

and, therefore, new and more powerful accelerators were built. Today, the principal role of the PS is to provide beams to these new machines (SPS, LHC). With a circumference of 268 meters, the PS has 277 conventional (room-temperature) electromagnets. It usually accelerates either protons delivered by the PS booster or heavy ions from the Low Energy Ion Ring (LEIR), at energy up to 25 GeV.

The PS main magnet system consists of a ring-shaped structure 200 m in diameter. This structure comprises 100 combined-function magnet units (MU), which are called because they combine the dipole and quadrupole magnetic fields in one magnet. For these reasons, they are able to bend and focus the particle beam. Each unit is composed of a focusing half-unit (F) and a defocusing half-unit (D). Between two subsequent magnet units, there is an interval called "straight section" (0) which is used for placing accelerating cavities, beam diagnostic devices, injection and extraction elements and magnetic lenses. The recurrent pattern is 'FOFDOD' (Fig. 2.3). A reference unit (MU 101) is located outside the tunnel in

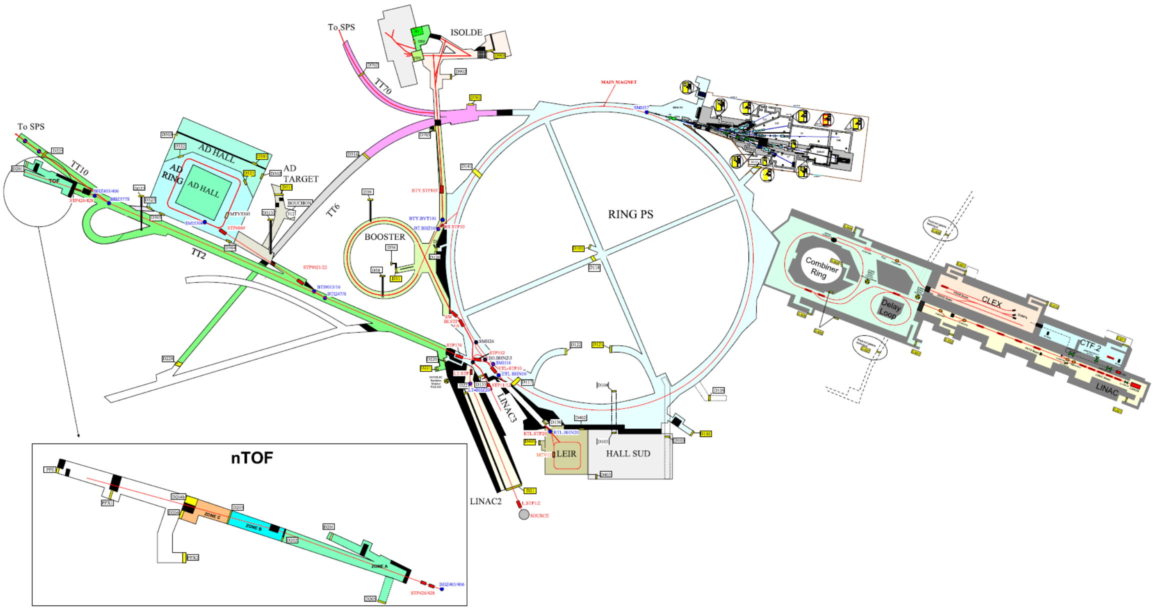

FIGURE 2.2: Proton Synchrotron complex layout

Circumference $[m]$	$2\pi 100$
Number of straight sections	100
Vacuum chamber type $[standard]$	elliptical
Standard vacuum chamber aperture $[mm]$	140×70
Maximum $\frac{dB}{dt}$ $[Gauss \setminus ms]$	21
Bare Tunes $Q_{x,y}$	$6.25 \setminus 6.28$
Bare chromaticities $\xi_{x,y}$	$\sim -0.8 \setminus -1.0$

TABLE 2.1: Main parameters of the PS machine

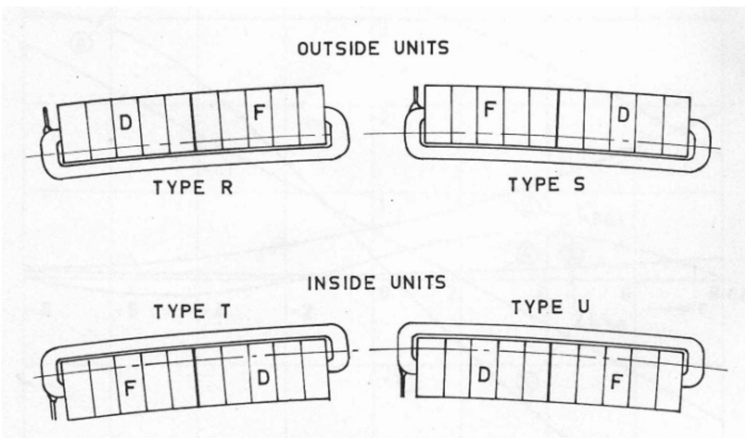

FIGURE 2.3: The recurrent pattern for inside and outside PS main magnets

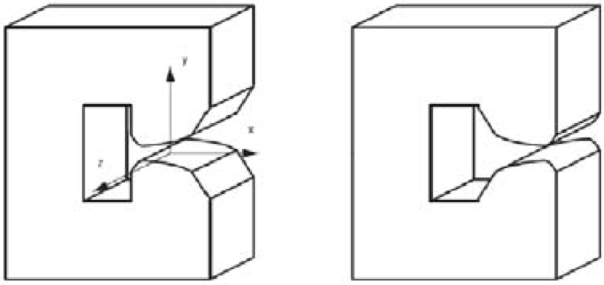

(a) Open and Closed single block

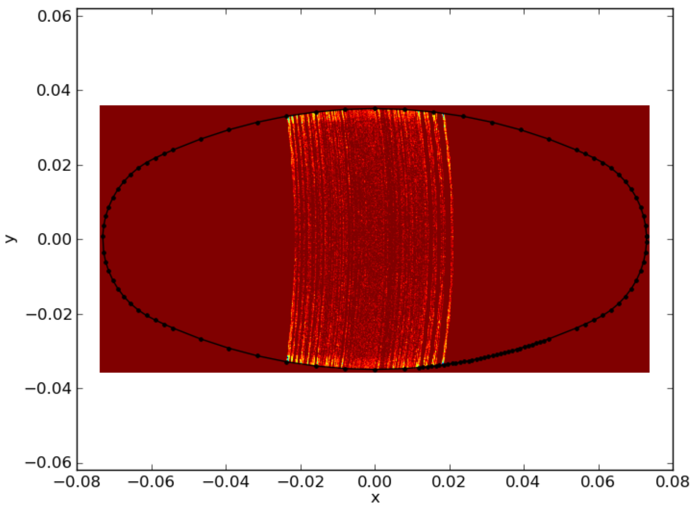

(b) Simulated magnetic field lines in a open single block

FIGURE 2.4: Combined function magnet units in the CERN PS

a dedicated air-conditioned room. Electrically in series with the other 100 units in the tunnel, it serves to produce reference signals for timing, beam control and field monitoring purposes. Each half-unit is composed of five adjacent magnet blocks, each 417 mm long. A block is a straight C-shaped structure of open or closed type (Fig. 2.4). Employing two different types of block, it is possible to produce the alternation of the gradient. In this way, the beam is focused both in the y-axis and in the x-axis along the ring. The ten blocks of each unit are powered by the same coil [22].

Beam	**LHC 25ns**
Proton kinetic energy $[GeV]$	25
Number of bunches	72
Bunch spacing $[ns]$	24.97
Number of protons per bunch	up to 1.1×10^{11}
Transverse emittance ε_n $[\mu s]$	3.0
Longitudinal emittance ε_l $[eVs]$	0.35
Bunch length at PS extraction $[ns]$	4

Table 2.2: Parameters of the LHC beams produced in the PS at extraction

2.1 The PS as LHC Injector

Nowadays, one of the main task of the PS accelerator is the production of LHC multi-bunch beams for physics experiment, according to the nominal mode of operation for the filling LHC (see Tab. 2.2). All LHC beams are produced using harmonics from the PSB. Nevertheless, up to 4 bunches can be sent per batch to the PS since the PSB consists of 4 superimposed rings. Until now, the LHC physics beams were produced in a double-batch transfer from PSB to PS using 4 + 2 rings.

In nominal conditions, the PS delivers beam to the SPS every 3.6 s in batches of 72 bunches spaced by 25 ns. The complete process is sketched in Fig. 2.6. Six bunches come from PSB are captured in two different cycles into PS. Here, they undergo a triple splitting and then, after acceleration to $26GeV \setminus c$, are again double splitted resulting 72 bunches into the SPS. In this way, it is possible to leave a 320 ns gap in the bunch train for the rise-time of the ejection kicker [23].

2.2 Electron Cloud effects in the CERN PS

EC effects have been observed at CERN PS during the last runs for the production of LHC type beams (2001), during bunch compression. The electron cloud induces distortions in electrostatic pick-up signals both in the PS ring and in the transfer line towards the SPS [24]. In 2006 transverse instabilities immediately before extraction were observed for short bunches [25], and in 2007 an EC test setup with

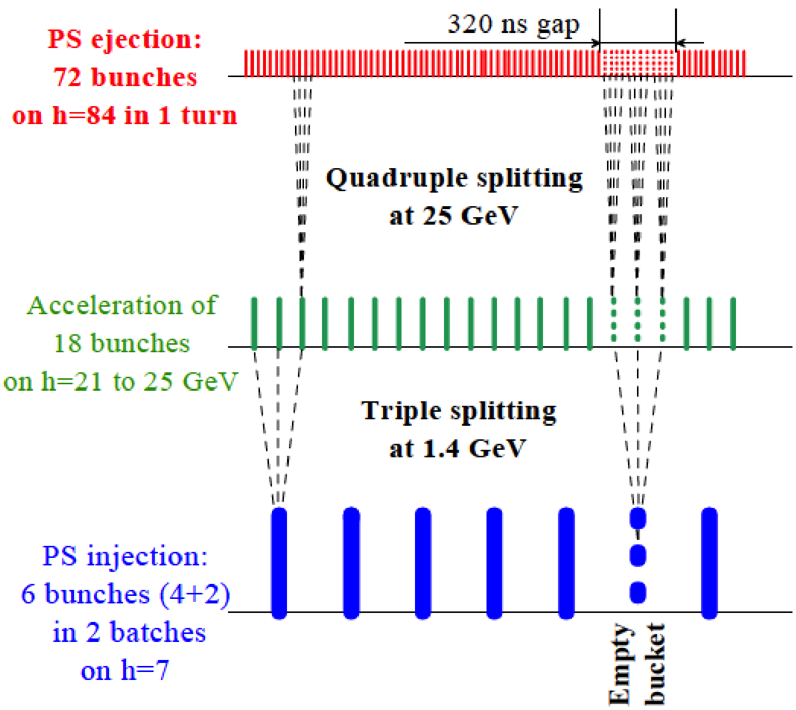

Figure 2.5: Generation of the nominal bunch for LHC 25ns

two shielded pickups was installed in one of the straight section of the ring and direct measurements could confirm the presence of EC in the vacuum chamber [26]. It is observed that EC is developing also in the main magnets but there is no direct confirmation since dedicated diagnostics will only become available after the 2013-2014 machine shutdown [26]. On the other hand with the present beam parameters, the EC does not represent a limitation for the production of LHC beams. Nevertheless, according to the high intensity and high brightness required by LHC Injectors Upgrade (LIU) project, several studies are carried out to develop a reliable EC model of the PS vacuum chamber, identify possible future limitations and find suitable countermeasure.

The EC built up happens only few tens of millisecond before the extraction, after the last bunch splitting when the final pattern with 72 bunches and 25 ns spacing is achieved (see Fig. 2.6 and Fig. 2.7). The reason for the absence of visible EC signature is that the beam does not interact with the EC for a long time. The

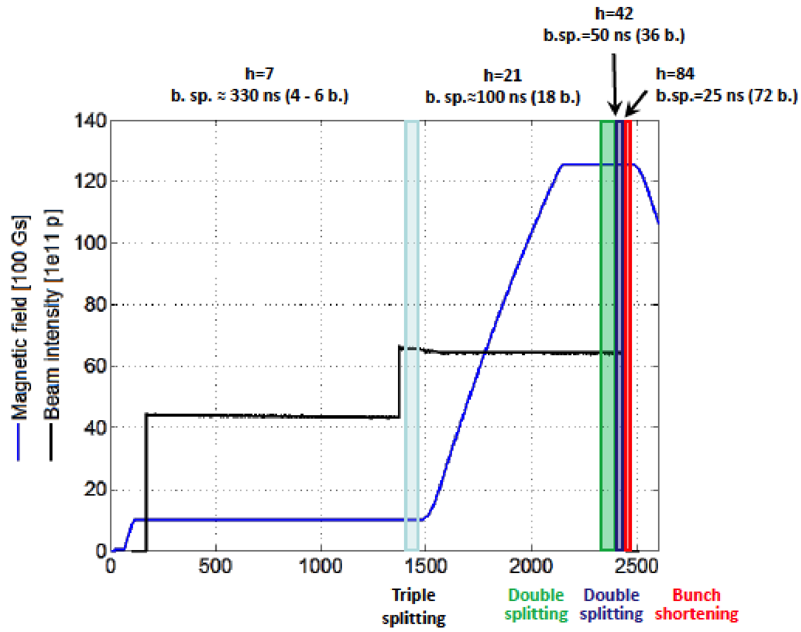

FIGURE 2.6: The machine cycle for the production of the LHC-type beam with 25 ns spacing in PS.

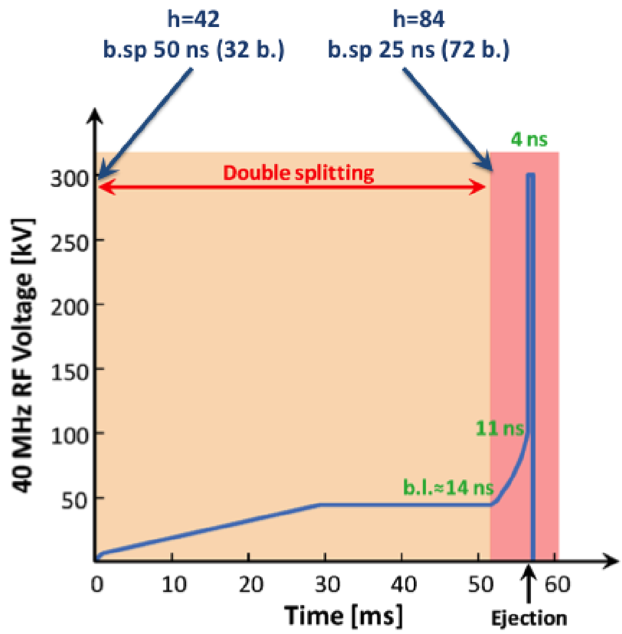

FIGURE 2.7: RF voltage program (40 MHz) during the last stages of the cycle for the production of the LHC type beams.The total (4σ) bunch length is reported in green. In the inset the evolution of the longitudinal profile of two bunches during the last bunch splitting (from 50 ns to 25 ns bunch spacing).

structure of the beam becomes prone to the production of EC only when the last bunch splitting is performed and the final pattern is achieved. As shown in Fig. 2.7, the last bunch splitting starts 57 ms before the extraction, with the ramp -up of the 40 MHz RF voltage, and it is completed less than 10 ms before the extraction, after the ramp-down of the 20 MHz RF system voltage [11]. At this point the bunches are about 14 ns long and they need to be shorted to 4 ns, as required by nominal SPS beam type. This is done in two step: 1) an adiabatic shortening, in which the RF voltage goes from 40 kV to 100 kV in 5 ms and the bunch length is about 11 ns and 2) a non adiabatic "bunch rotation" performed by the RF voltage up 300 kV to reduce the bunch length to values of about 4 ns. Actually, simulations and measurements have shown that the EC build up in the PS is very sensitive to bunch length variations; the density is highest for short bunches. Some modifications were introduced in the RF voltage program in order to minimize the interaction of the beam with EC without introduce any important degradation of the beam quality at the extraction from the PS [27].

2.3 The PS electron detector in MU98

The EC detector is used to measure the electron flux through a grid of holes on the vacuum chamber surface. Electrons are collected by a shielded electrode and measured as a current signal.

During the 2013-2014 machine shutdown (LS1), a new electron cloud detector has been installed in one of the PS main magnets to study the EC effects in strong magnetic field condition, with intensity more than 1 T (see Fig. 2.8). The pick-up is made by a ceramic block shielded from the main chamber with a 0.2 mm thick stainless steel sheet hosting of a series of holes whit 1 mm diameter and 2 mm pitch (see Fig. 2.10). The ideal position for a detector should be on the middle of the vacuum chamber, placed on thetop or the bottom part of the chamber (see Fig. 2.4). Nevertheless, due to space limitation in the PS main magnet, the flange is inclined by 30 degrees with respect to the bottom part of the beam pipe. The

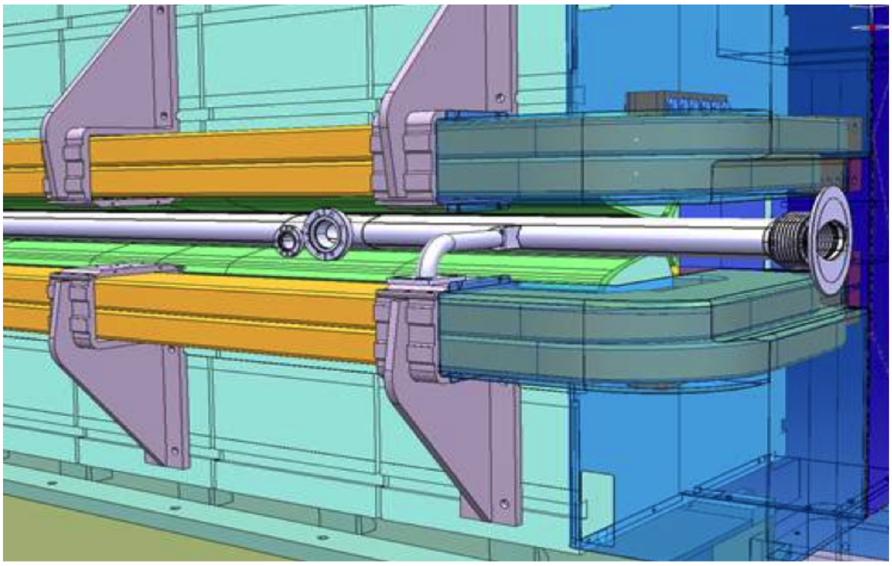

Figure 2.8: Location of the flanges for the new electron cloud monitors within a main magnet. The big one is used for the installation of shielded pick-up. The small one is an optical window to measure the electron-photon emission. The main magnet unit is represented in yellow (Courtesy of T.Capelli).

distance between the end of the pick-up and the vertical axis of vacuum chamber is 1.2 cm (see Fig. 2.9). Therefore, for a good quality of the signal it might be necessary to displace the beam inside the chamber [28].

The analysis of the simulated signal for different beam position will be discussed in the next Chapter.

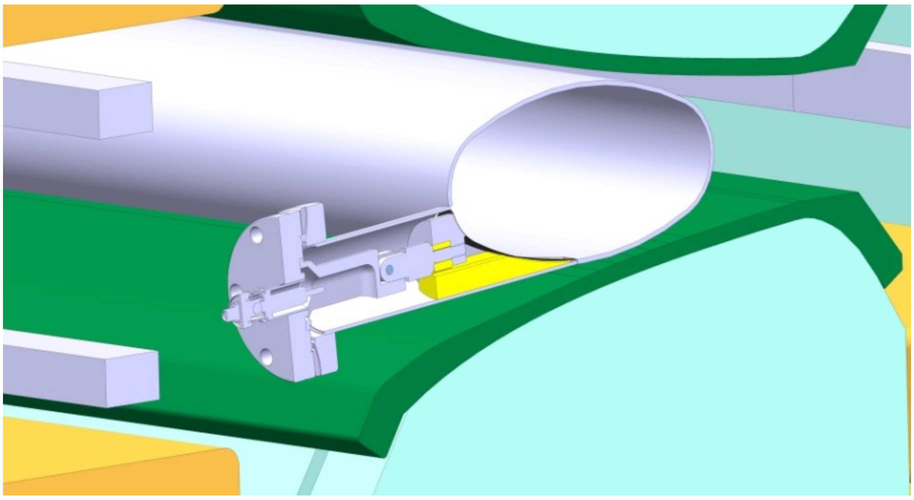

(a) 3-D design

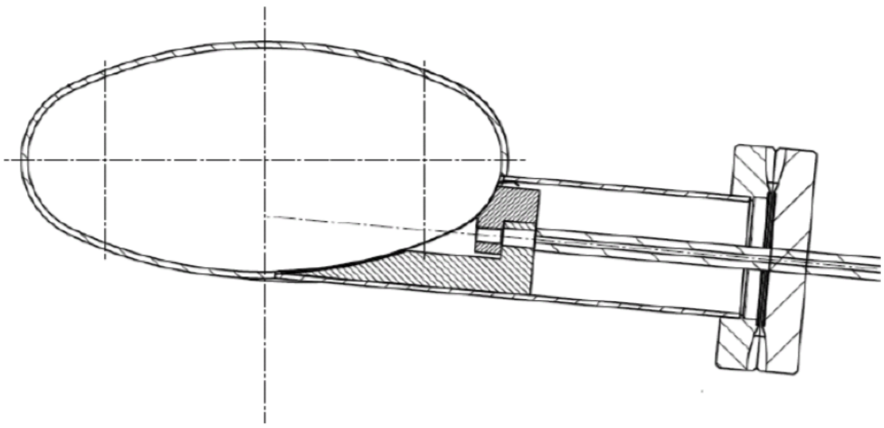

(b) Project design

Figure 2.9: Position of a pick-up in the vacuum chamber

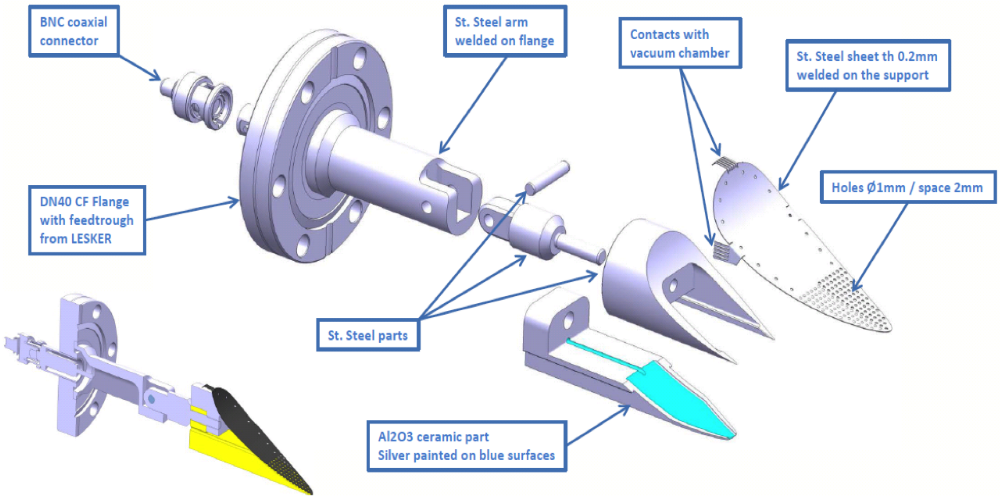

(a) 3-D design of pick-up

(b) Real pick-up

FIGURE 2.10: Electron pick up for MU98 vacuum chamber (Courtesy of T. Capelli and C.F Eymin)

Chapter 3

Simulations of Electron Cloud detector in PyECLOUD

In the previous chapter, it was pointed out that the CERN PS is a key-accelerator in a CERN complex with a central position in the LHC accelerator chain. As the intensity per bunch and high brightness have increased over the years, limitations directly related to them were discovered. Therefore, an effort has to be done to understand these limitations and several studies are carried out to find suitable solutions.

The purpose of this chapter is to describe the main features of the new EC detector installed in the PS machine and improve our general understanding on EC effects. An intensive simulation campaign has been conducted in order to determinate the expected EC signal under different operating conditions.
For the first time, PyECLOUD was used to simulate the behavior of electrons in presence of an EC detector. Therefore, the first step was to consider an EC device for which was possible to compare new PyECLOUD results with previous ones obtained with ECLOUD code.
Later on we performed the implementation of the PS EC detector in PyECLOUD. The presence of a strong non uniform magnetic field and the necessity of taking into account the actual chamber shape, resulted in several numerical issues mainly

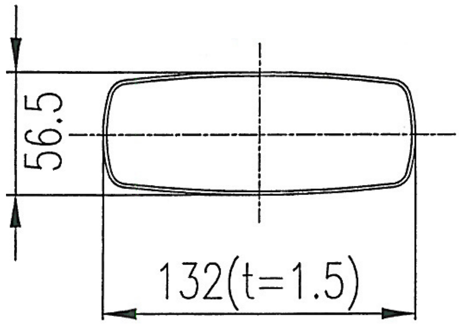

(a) Magnetic benders dipole chamber (MBB)

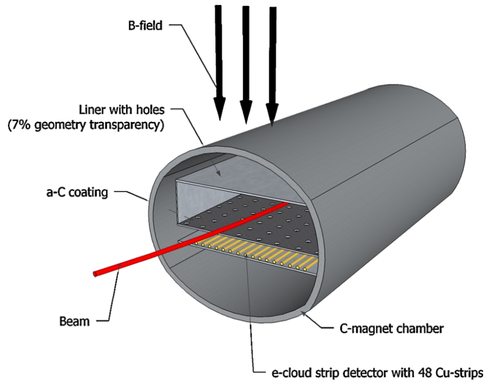

(b) Schematic view of the strip detector (courtesy of C. Yin Vallgren)

FIGURE 3.1: Multi−strip detector installed in the CERN SPS

related to the computation of the MPs motion in the magnetic field. They were solved by thoroughly optimizing of the numerical settings of the simulator.

Finally, the results of simulations obtained under different beam conditions (bunch length, bunch intensity and beam radial position) were analyzed.

3.1 Test Case: SPS strip detector

EC monitors (ECMs) are installed in the SPS dipole magnets to study the EC build up also in presence of low SEY materials. These ECMs are equipped with liners having the same cross section as the vacuum chamber of the SPS bending magnets. A magnetic field variation from 0 to 2000 Gauss (1200 Gauss is the SPS injection value) can also be applied. The liner has length of 1050 mm featuring by a grid of holes (2 mm diameter and 6 mm pitch) providing a geometrical

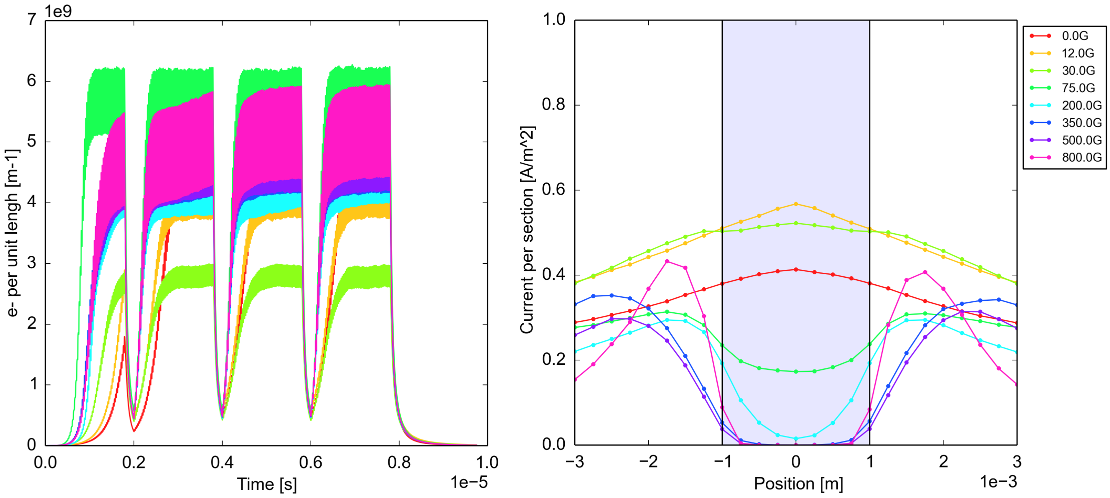

(a) Electron Cloud build up for different value of magnetic field. According to simulations, EC effect can occur even at low magnetic field

(b) The presence of holes depletes the EC at high fields. The blue region defines the contours of hole.

FIGURE 3.2: Influence of holes on the electron distribution inside the chamber

transparency of 7% [29]. The holes are drilled directly on the side of chamber facing the detector.

A multi-strip detector consisting of 48 copper strips parallel to beam axis, with 1.2 mm pitch, is used to collect the electrons escaping through the holes. These holes are arranged in rows inclined with respect to the beam direction in order to avoid any systematic dependence of the signal generated by an electron stripe on its position.

Several PyECLOUD simulations have been performed in order to analyze the EC behavior in the detector. The results show that EC growth is strongly dependent on the field of the dipole magnet as well as the presence of holes.

PyECLOUD simulations show that the EC effect can occur already at low magnetic field. For higher fields, the cyclotron radius of electrons tends to shrink. As a consequence, no multipactor process takes place inside the holes and electrons come only from the edges.
This effect is shown in the Fig. 3.2 and Fig. 3.3.

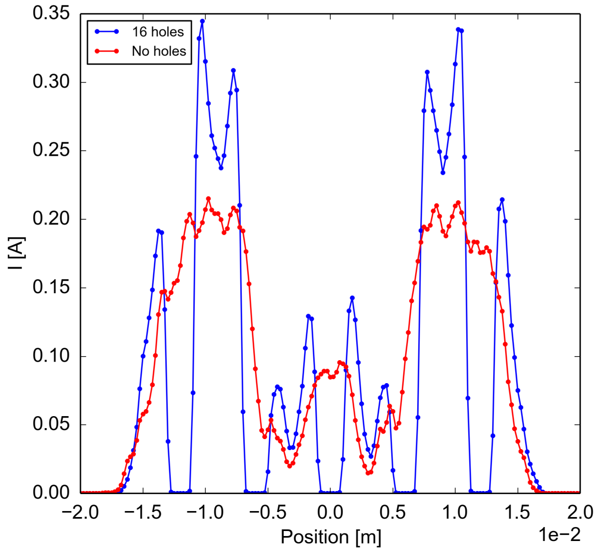

FIGURE 3.3: Distribution of electrons with and without holes for strong magnetic field. The EC is suppressed at the holes location but gets enhanced elsewhere due to the suppression of the electron space charge.

The other important aspect that was investigated is how the presence of the holes influences the SEY threshold. Looking at Fig. 3.4 a), we can observe that for high magnetic field the electron density is basically the same both with and without holes. This is due to the fact that, being the electrons constrained to move around the field lines, the dynamics of the EC is slightly perturbed by the presence of the holes.

On the contrary, for low magnetic field the SEY threshold is strongly affected and moves from 1.3 without holes to 1.5 with holes. It was demonstrated that gradually removing the holes from simulation, the value with holes gently converges to the unperturbed case. This is shown in Fig. 3.4 b).

The new PyECLOUD simulations were compared against previous studies carried out with the ECLOUD code. The same bunch length, bunch intensity, SEY value and machine parameters were considered. The results are presented in Fig. 3.5 showing a good agreement between the two cases and confirm the correct implementation of the detector in PyECLOUD.

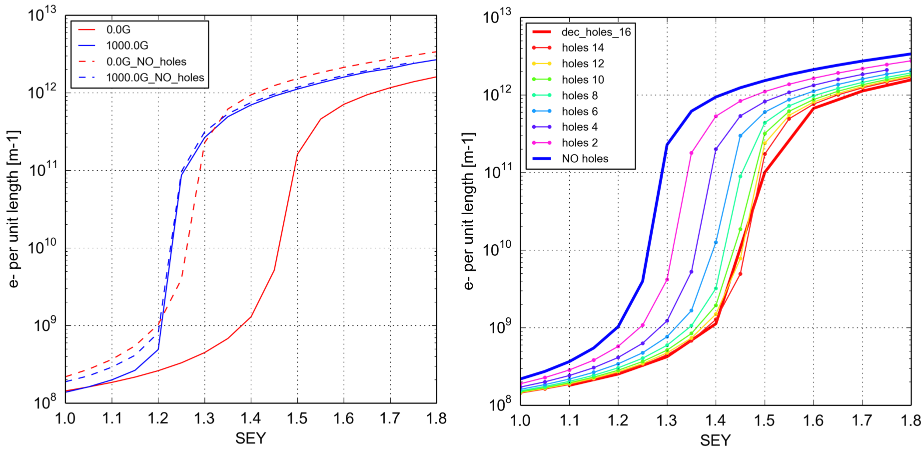

(a) SEY thresholds for different values of magnetic field

(b) Study of threshold convergence for low magnetic field

Figure 3.4: Influence of holes on the SEY threshold for multipacting

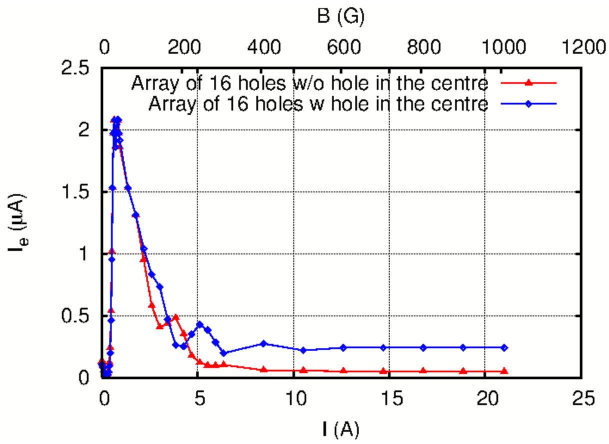

(a) Previous ECLOUD simulations results

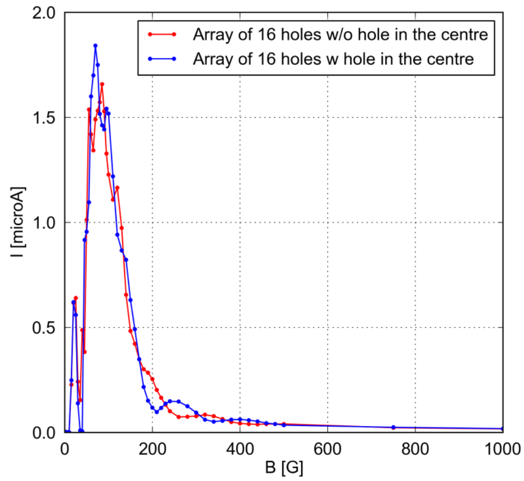

(b) New PyECLOUD simulations results

Figure 3.5: Comparison between PyECLOUD and ECLOUD simulations for an SPS multi-strip detector

3.2 Implementation of the PS EC detector in PyECLOUD

In this section, we will discuss the modeling in PyECLOUD of the EC detector placed in one of the main combined function magnets in the PS.
Starting from the realistic geometry of the beam pipe (see Fig. 3.6 a)), the surface of the chamber was reproduced approximated with a polygon as shown in Fig. 3.6 b). It is made of adjacent segments with different size and SEY.

The red region of the chamber corresponds to the detector. In PyECLOUD, the holes are modeled as segments with zero SEY on the chamber wall since they don't produce secondary electrons. For segments which compose the rest of the chamber, the SEY has been scanned in a range between 1.3 to 1.5, according to the possible values for the technical surface. These segments are represented in blue.

For all simulations, it was necessary to set some initial parameters, according to the features of the machine and to the case which one intends to simulate. The first step has been the check of the numerical convergence with respect to the numerical parameters.

In the past, the PS simulations were performed using a semi-analytical tracking method (StrongBgen) to solve the electrons equations of motion in a generic magnetic field. Nevertheless, this algorithm was found to be reliable for dipole fields but not sufficiently accurate in case of quadrupole fields [30]. Indeed, the semi-analytical method which allows to use a time step longer than the cyclotron radius is not suitable for long term electron tracking. In presence of a magnetic gradient, the build up simulations require a long term accuracy since electrons can survive during several bunch passages. For this reason, a Boris tracker has been also implemented in PyECLOUD. In order to check the robustness of this algorithm also for the magnetic field generated by the combined function unit, simulations with both methods have been performed and compared.

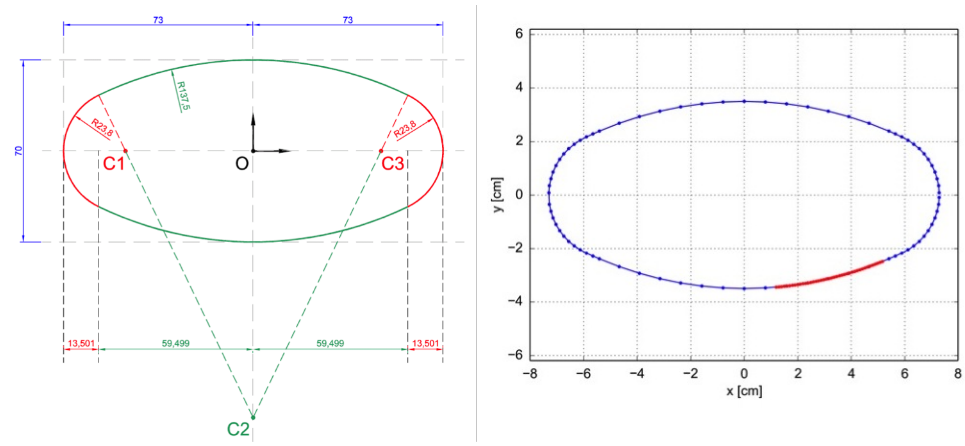

(a) Realistic geometry of the PS beam pipe (b) Implementation of the PS chamber in PyECLOUD

FIGURE 3.6: The PS beam pipe model

Fig. 3.7 shows a curios effect which was pinned down: the semi-analytical method introduces an unphysical drift of the electron distribution in the transverse plain. Performing the same simulations with Boris Tracker, this effect disappears and the EC signal through the holes is correctly evaluated.

The implementation of this method required a study of convergence to identify a reasonable value of time steps and number of Boris substeps, which is the number of times for the computation of electrons tracking, in order to provide a good balance between accuracy and an acceptable simulation time. As it is shown in Fig. 3.8, two different cases are analyzed. Fixing the substep to 30 and changing the main time step from 5 to 25 ps, the electron distribution does not change significantly and also the current through the holes is not affected. Fixing then the time step to 25 ps and changing the substep from 5 to 30, it was found that the electron distribution is again the same in all these cases, but the current through the holes only converges for a number of substeps larger than 10.

The last aspect that was investigated is the influence of the initial distributions of primaries on the simulation results.

In Fig. 3.9, three different configurations are studied. In the first two cases (see Fig. 3.9 a) and b)), primaries are generated by gas ionization mechanism and they are distributed mainly in the middle of the chamber. In both cases, the final electron distribution tends to be noisy and evolves in three stripes with some suppression in between. Nevertheless as it is shown in Fig. 3.9 b), increasing the initial number of MPs it is possible to obtain a slight improvement of this profile. If the same large number of MPs is uniformly distributed in the cross section of the beam pipe (see Fig. 3.9 c)), we can observe that the electron distribution appears smoother and the noise is attenued. This has also a positive impact on the estimation of the current through the holes.

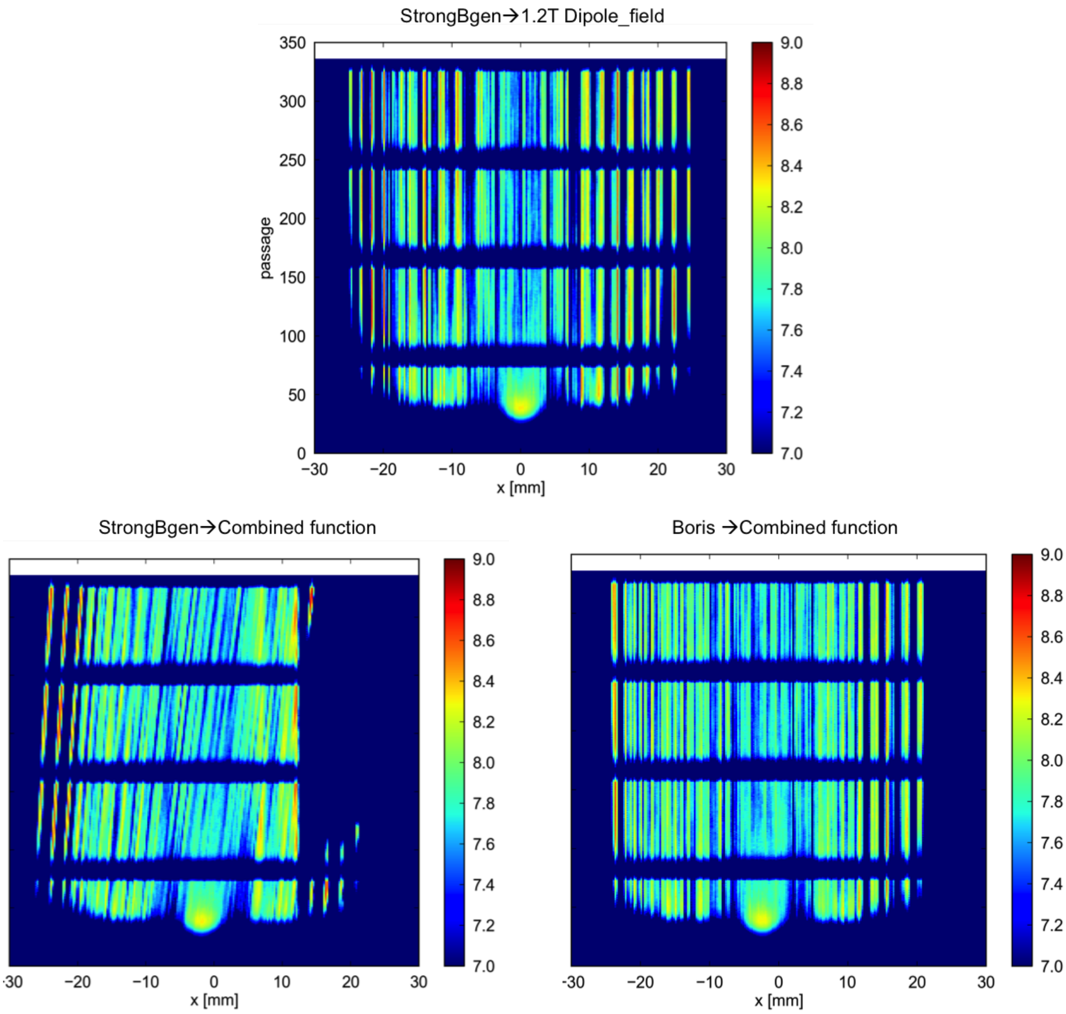

FIGURE 3.7: Computation of the electron distribution in different magnetic field condition. Diagrams evaluate the number of e- which impact against the wall for bunch passage in each beam pipe's slice. Top: Generic algorithm applied for a dipole field (1.2 T). Top right: General algorithm applied for a combined function magnet. Bottom right: Boris algorithm applied for a combined function magnet

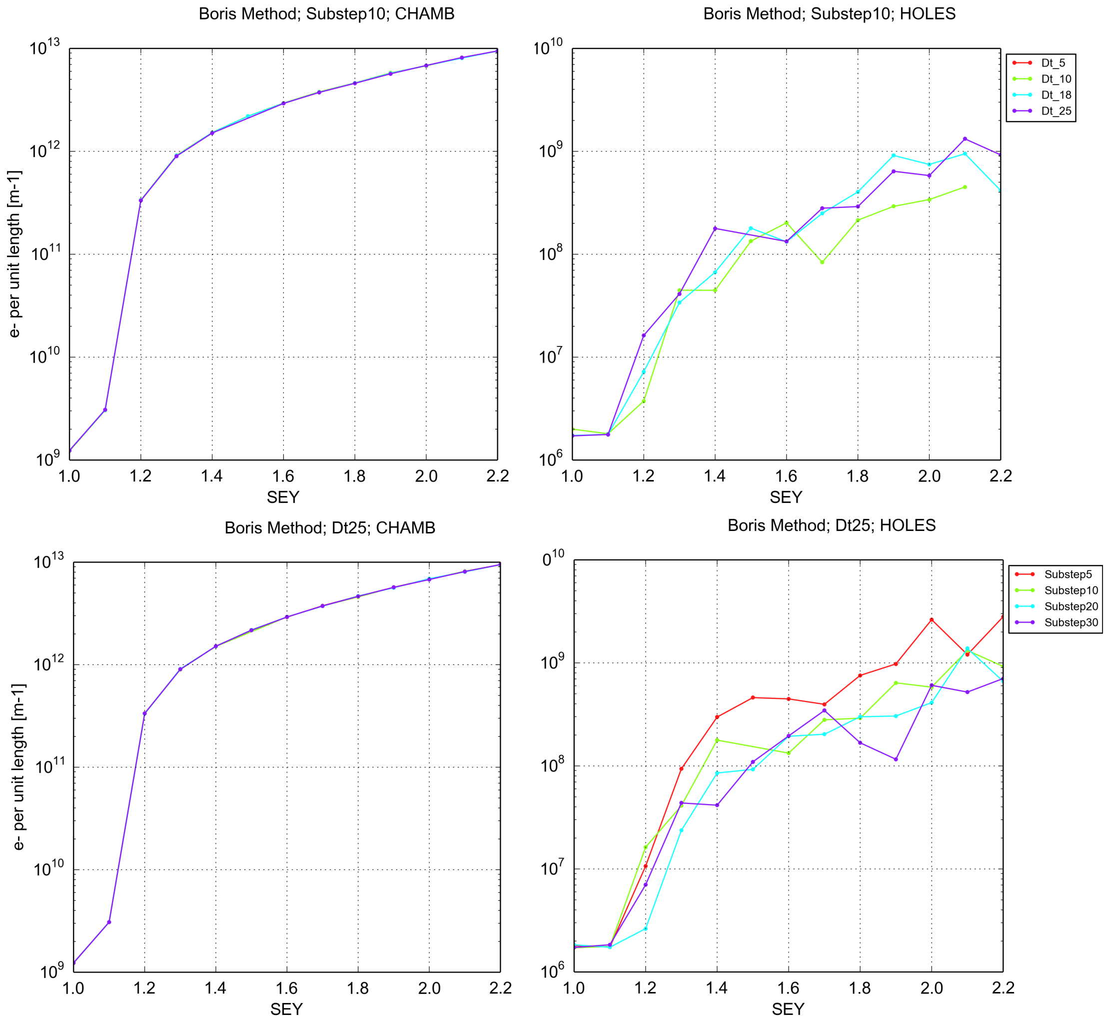

FIGURE 3.8: Study of Boris method convergence. Diagrams represent the current both through the chamber and through the holes for different time step (bottom) and different number of substeps (top)

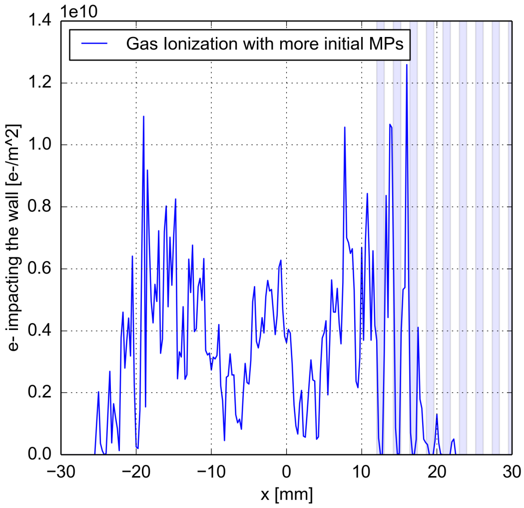

(a) MPs generated by gas ionization mechanism. Lower number of initial MPs.

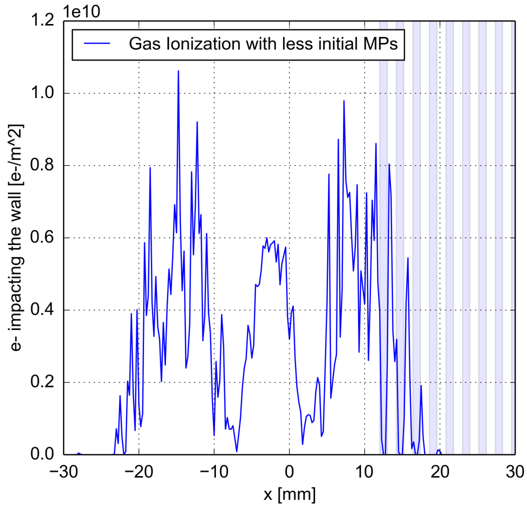

(b) MPs generated by gas ionization mechanism. Larger number of initial MPs.

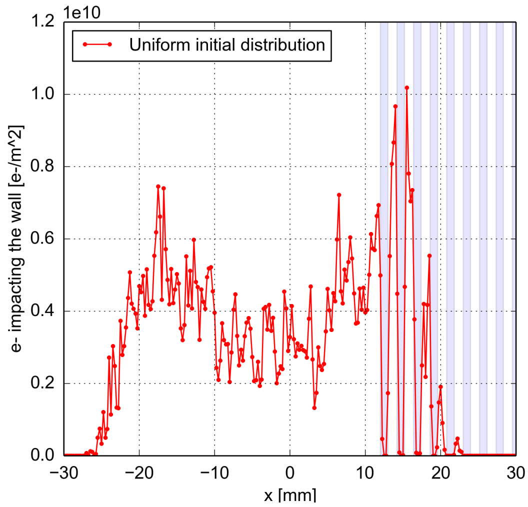

(c) Larger number of inial MPs uniformly distributed inside the chamber

FIGURE 3.9: Influence on the simulation results of the initial number of MPs and their distribution inside the chamber. Blue stripes represent the holes.

3.3 Parametric simulation studies

The dependence of the EC buildup on the beam conditions has been studied with several PyECLOUD simulations. In this study, the relevant ranges of bunch length and population and radial position of the beam were covered: [4-16] ns, [10^{11}, $2.5\text{x}10^{11}$] ppb and [-3, 3] cm, respectively. The bunch length range simply corresponds to the values really covered during the last part of the cycle for the LHC 25 ns beam production from right after the last bunch splitting until extraction. The bunch population range includes reasonable values which can be reached nowadays and extend to the future values foreseen by the LHC Injectors Upgrade (LIU). Finally, the radial position range corresponds to the maximum values for which is possible to shift the beam inside the chamber.

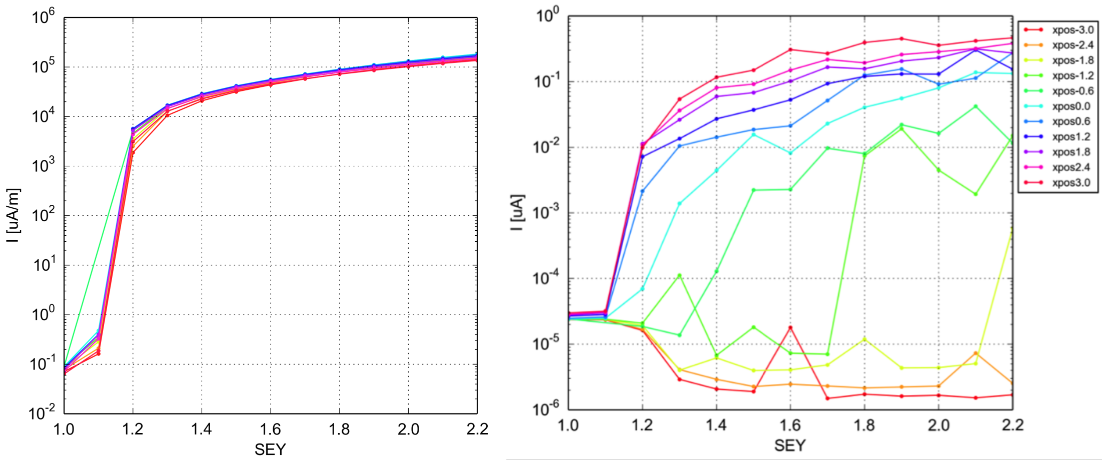

(a) EC expected signal on the whole chamber surface

(b) EC expected signal through the holes

FIGURE 3.10: PyECLOUD simulations for the study of the EC threshold. EC line density as a function of the SEY for different beam positions inside the chamber. Left: the SEY threshold around all chamber is 1.2. Right: in order to obtain a SEY threshold comparable to the one of the whole chamber the beam should be displaced by at least 1 cm from the center.

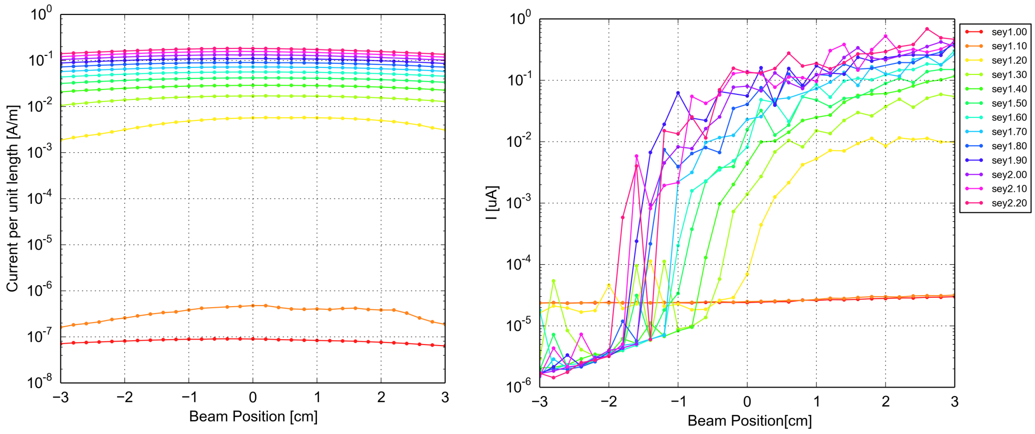

(a) Expected current on the whole chamber's surface

(b) Expected current through the holes

FIGURE 3.11: Influence of the beam position on the expected signal for different SEY. Left: the electron flux is not strongly influenced by the beam position, but only by the SEY. Right: in this case, the current depends both on the SEY and beam position.

3.3.1 Simulation scans for different beam radial position

Figures 3.11 and 3.12 show that the capability of the detector to measure an acceptable signal is strongly dependent on the beam radial position within the chamber which can be changed operationally through local orbit bumps.

In particular, Fig. 3.11 shows the EC current through the detector as a function of radial position of the beam and SEY parameter. We can observe that the beam should be sufficiently close to the region of the detector to measure the EC signal.

The fig. 3.12 shows the horizontal distribution of electrons as function of radial position for a value of SEY equal to 1.6. Six different configurations have been considered. In this way, it is possible to compare the results and identify the most suitable configuration.

3.3.2 Simulation scans for different bunch length

The purpose of these simulation scans is to study how the multipacting threshold changes for different bunch length. In particular, three values of bunch length

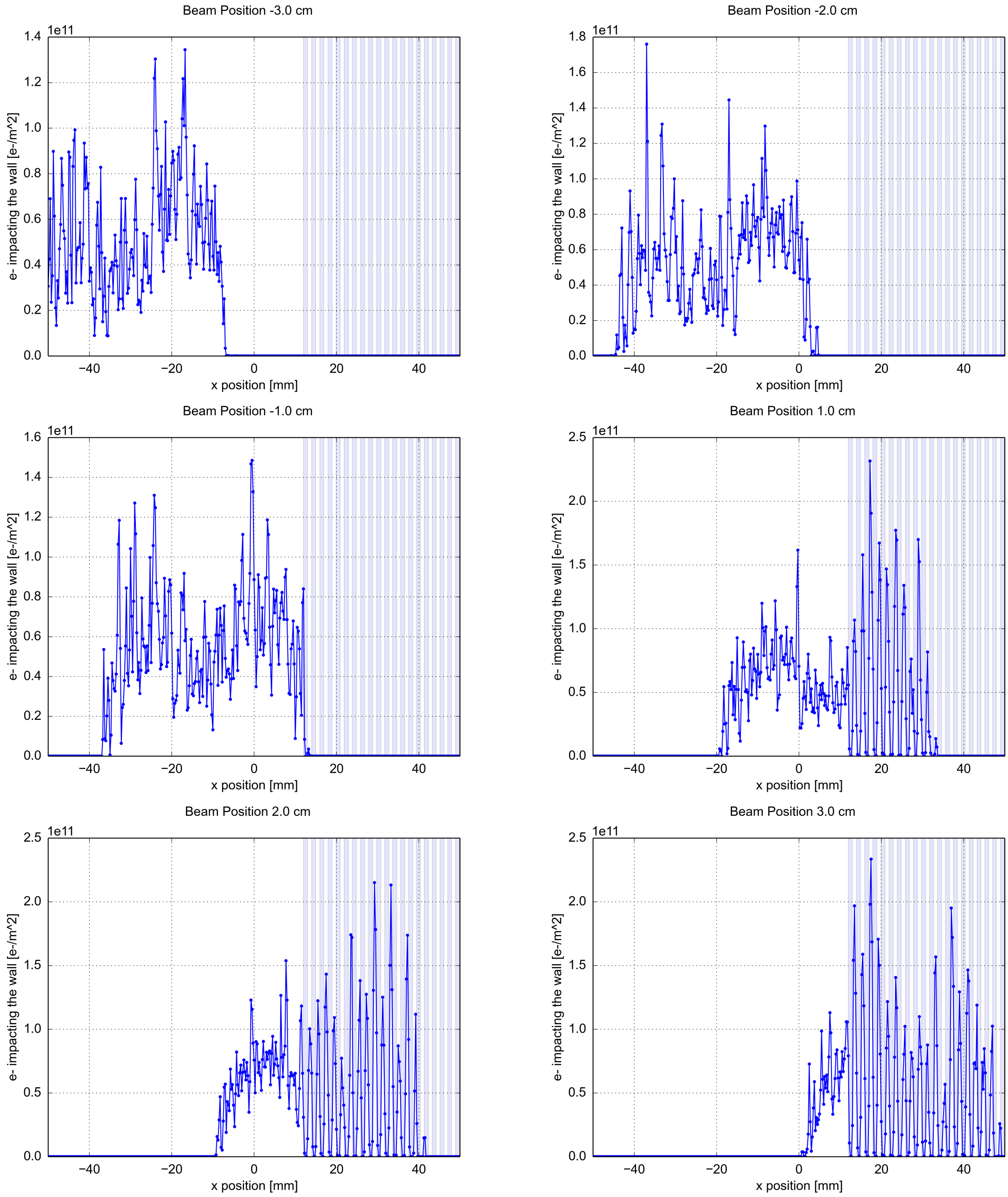

FIGURE 3.12: Horizontal distribution of electrons for different beam position inside the chamber. SEY equal to 1.6, the capability of the EC detector to measure an acceptable signal is strongly dependent on the beam position.

were considered (14, 10 and 4 ns). For each of them, the EC signal is simulated as a function of δ_{max} and all range of bunch population is covered.
The results of these studies are summarized in Figs. 3.13, 3.14 and 3.15.

The EC build up has been simulated for two different radial position of the beam (at the center and 1 cm from it). For all cases, the electron flux is monotonically increasing as a function of the bunch length for all the simulated SEY values. Comparing Figs. 3.13, 3.14 and 3.15, we can observe that shorter bunches correspond to lower multipacting thresholds. This value may even decrease when increasing the bunch intensity.

3.3.3 Simulation scans for different bunch population

According to the results presented in the Sec. 3.3.2, several simulation scans have been done for different values of bunch intensity.

Here, we report the EC build up as function of δ_{max} and bunch length for two different beam positions.
The values of bunch populations that were considered are: 1.30x10^{11} and 2.50x10^{11} ppb. The fist one is the nominal value which is used for the LHC beam production, while the other one is future value of the LIU project.

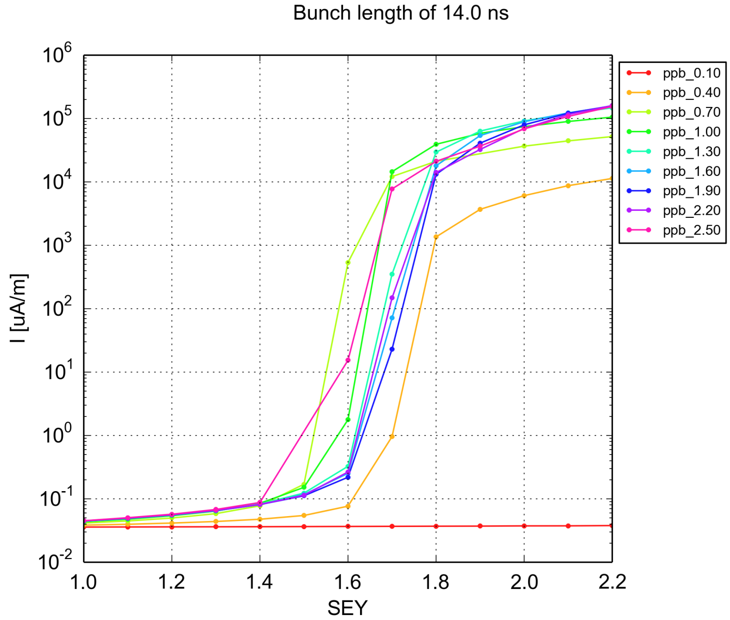

(a) Expected current on the whole chamber's surface

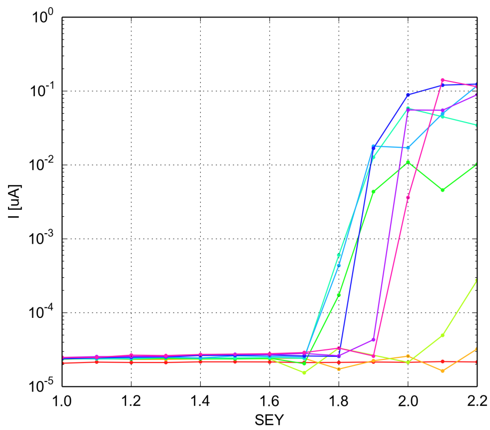

(b) Expected current through the holes- Beam position: Center

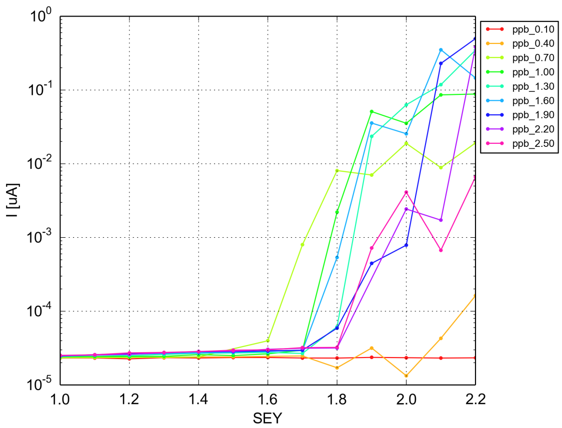

(c) Expected current through the holes- Beam position: 1 cm

Figure 3.13: PyECLOUD simulations for the study of the EC threshold. EC line density as a function of the SEY for different bunch population and for two different beam position inside the chamber. The bunch length is fixed to 14 ns, this is the value after the second double splitting.

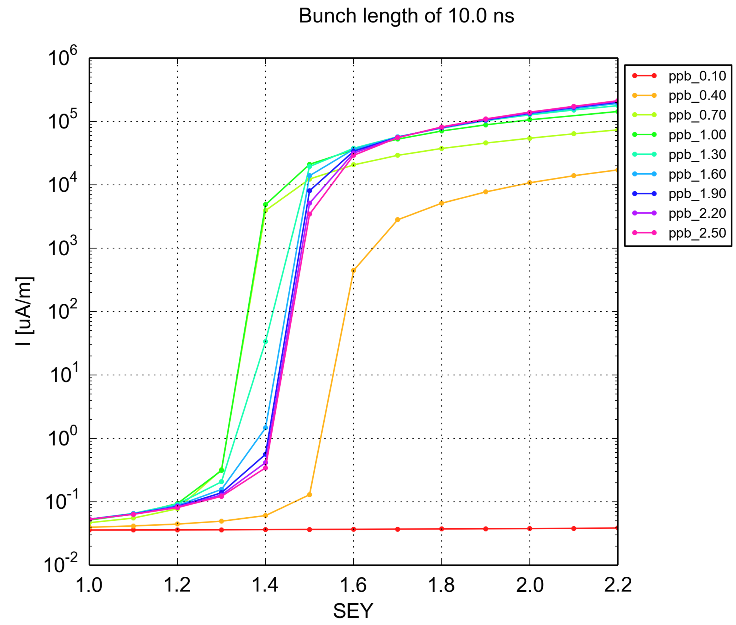

(a) Expected current on the whole chamber's surface

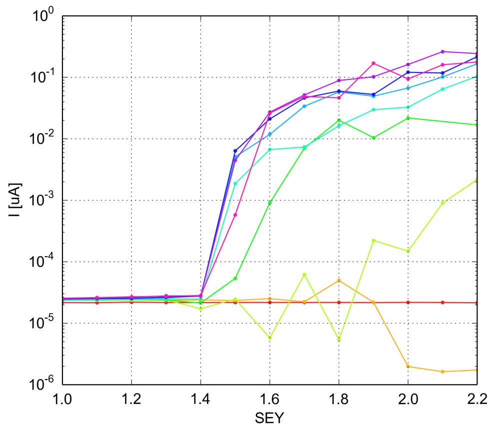

(b) Expected current through the holes- Beam position: Center

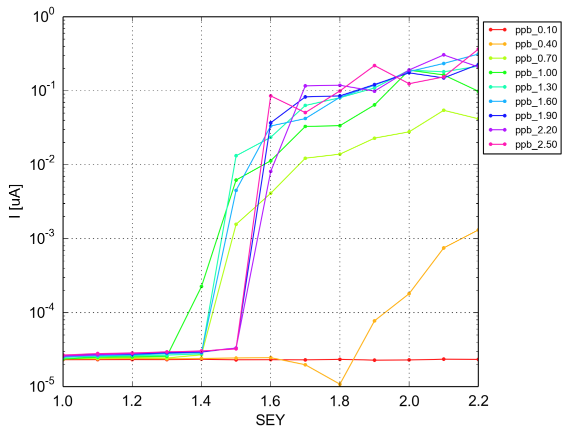

(c) Expected current through the holes- Beam position: 1 cm

FIGURE 3.14: PyECLOUD simulations for the study of the EC threshold. EC line density as a function of the SEY for different bunch population and for two different beam position inside the chamber. The bunch length is fixed to 10 ns, this is the value after the adiabatic bunch shortening.

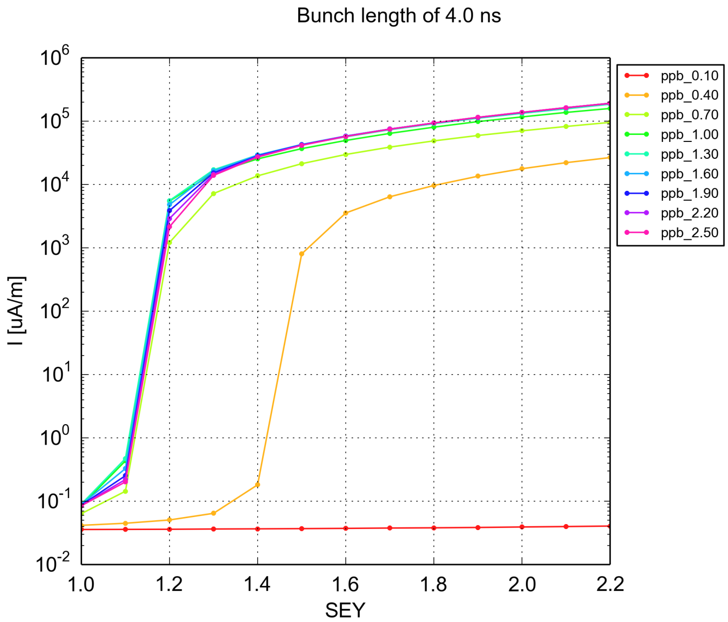

(a) Expected current on the whole chamber's surface

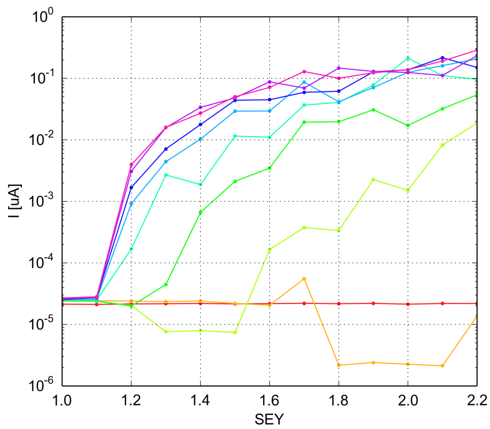

(b) Expected current through the holes- Beam position: Center

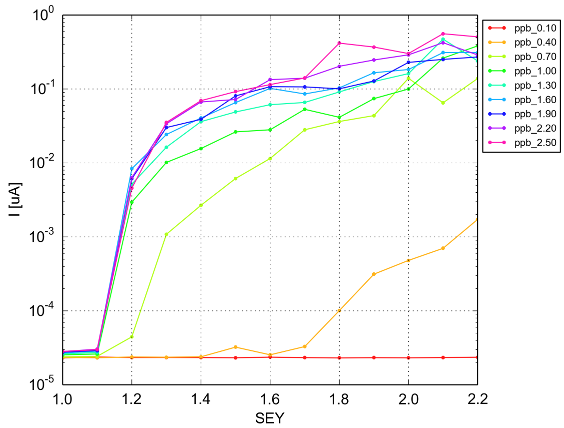

(c) Expected current through the holes- Beam position: 1 cm

FIGURE 3.15: PyECLOUD simulations for the study of the EC threshold. EC line density as a function of the SEY for different bunch population and for two different beam position inside the chamber. The bunch length is fixed to 4 ns, this is the value at extraction.

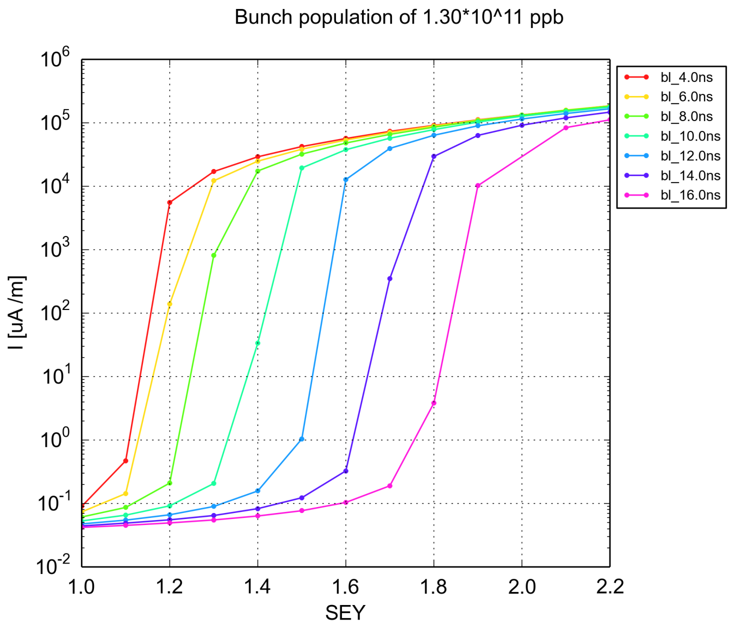

(a) Expected current on the whole chamber's surface

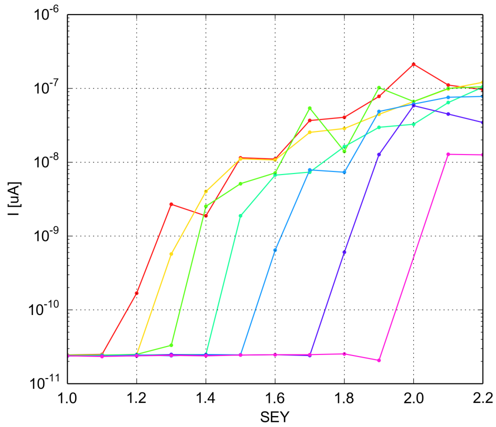

(b) Expected current through the holes- Beam position: Center

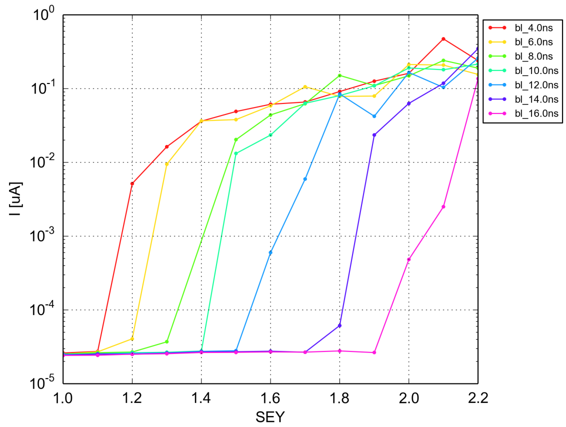

(c) Expected current through the holes- Beam position: 1 cm

FIGURE 3.16: PyECLOUD simulations for the study of the EC threshold. EC line density as a function of the SEY for different bunch length and for two different beam position inside the chamber (at center and at 1 cm from the center). The bunch intensity is fixed to 1.30x10^{11} ppb.

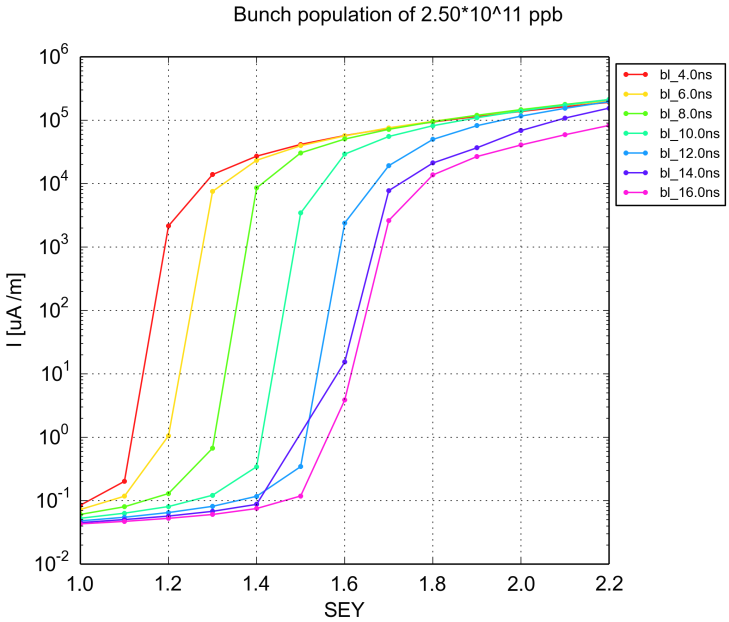

(a) Expected current on the whole chamber's surface

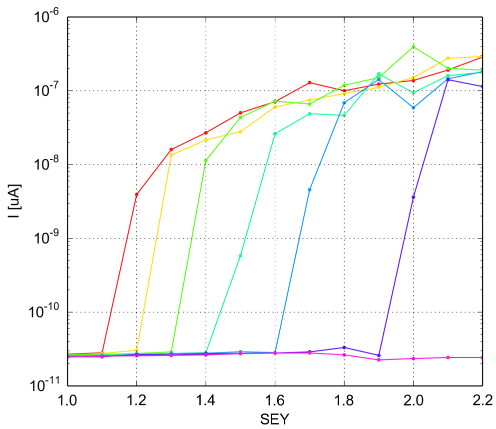

(b) Expected current through the holes- Beam position: Center

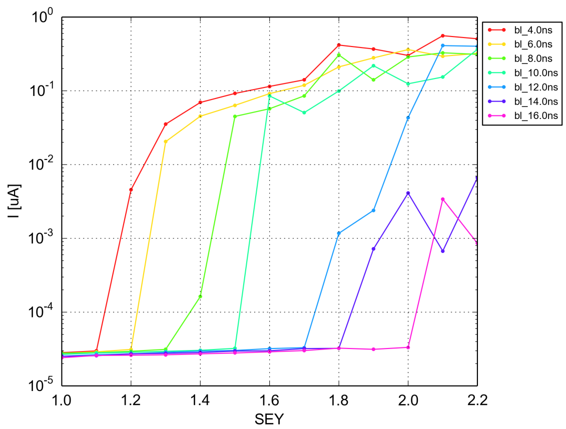

(c) Expected current through the holes- Beam position: 1 cm

FIGURE 3.17: PyECLOUD simulations for the study of the EC threshold. EC line density as a function of the SEY for different bunch length and for two different beam position inside the chamber (at center and at 1 cm from the middle). The bunch intensity is fixed to 2.50x10^{11} ppb.

Chapter 4

New EC mitigator materials for particle accelerators

In the previous chapters, EC effects in the CERN PS ring have been discussed and addressed with several numerical simulations since they represent the main limitation for high intensity particle accelerators. For this reason, a great effort has been recently devoted to the search of new strategies for EC mitigation.
As already said, one of the most important parameters that defines the importance of EC effects on the beam quality is the number of electrons produced by the accelerator walls when they are hit by other electrons. The SEY value, its time stability and its dependence on primary electron dose and energy represents indeed a crucial issue and an essential ingredient to predict and mitigate these detrimental effects.

Recently, different strategies to produce intrinsically low SEY surfaces have been studied and applied [19]. One such proposal is to reduce the SEY value by macroscopic geometrical modification of the accelerators walls, machining triangular or rectangular grooves on the otherwise flat accelerator wall surface.
The expected SEY reduction is based on some considerations:

- primary electrons have an energy distribution peaked at very low kinetic energy;

- the angular distribution of primaries is maximum at normal emission and it significantly decreases at grazing angles;
- the presence of a magnetic field will enhance the SEY reduction due to the additional spinning of the emitted electrons along the field lines within the grooves.

According to this, when electrons emitted from the surface at grazing incidence see the beam, and the ones emitted at normal incidence are shadowed by the surface itself, a net reduction of the SEY value can be achieve. Much work was dedicated to study these strategies and different types of macroscopically machined grooves have been theoretically analyzed, produced and successfully measured [31–33].

In the present chapter, it will be described a completely different material: Cu foams. Such materials, more and more diffuse in aerospace and automotive technology, are nowadays easily available from the market and are produced by several technologies.
Several experimental studies were required in terms of SEY, PY, vacuum behavior and their impact to impedance budget in order to finally qualify them as a mature technology to be applied into accelerator system [1, 34].
In the present work, it will be discussed the experiments performed at the Material Science INFN-LNF laboratory of Frascati (Roma) and at CERN.

4.1 Open cell metal foam

Due to its morphological properties, Cu foams represent an interesting candidate for materials to be use as beam screens of high intensity SR accelerators.
Its morphologic form may help reduce the effective SEY of the chamber, mitigate the EC build up and related instabilities [1].
The typical foam is a highly connected trabecular structure of solid metal filaments, which encircle the pores (see Fig. 4.1).

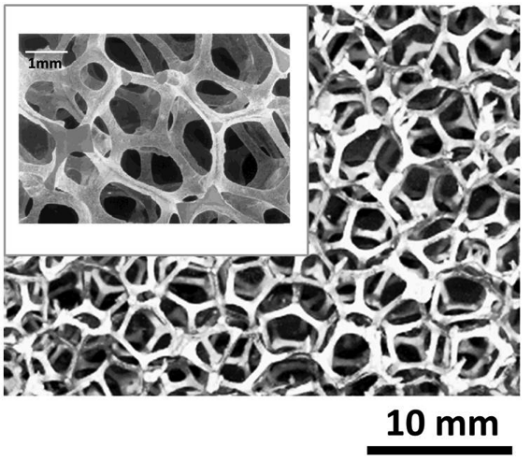

Figure 4.1: A typical open cell Cu foam at two different viewing scales

Compressive strength [MPa]	0.9
Tensile strength [MPa]	6.9
Shear strength [MPa]	1.3
Elastic modulus (compressive) [MPa]	7.3x10^2
Elastic modulus (tensile) [MPa]	1x10^2
Shear strength [MPa]	2.8x10^2
Specific heat [J/g]	0.38
Bulk thermal condition [W/m ℃]	10.1
Thermal expansion coefficient [1/℃]	1.7x10^-5
Bulk resistivity [Ω/m]	6.5x10^-7
Melting point [℃]	1100

Table 4.1: Structural properties of Cu open cell metal foams [1].

They can be produced by different processes but with the same scope to make the structure of Cu foams highly gas-permeable with remarkable mechanical, electrical and thermal properties shown in Tab 4.1. It is studied that the outgassing of foam walls can be better by a factor 10 compared to the best slotted walls, thanks to their mechanical-structure foams should be adequate to resist eddy currents and their surface resistance is very low [1]. Usually, the solid metal is only a small fraction of the total volume (typically, some 10% or less). The key morphological parameters are: pore size (typical diameter between 10^-1 and 10^-3 mm) and porosity (typical volume fraction of pores is 0.8-0.99).Interestingly, it is possible to model such structures to simulate their behavior using, as building blocks, equal-sized (and possibly unequal shaped) pores by using the Weaire-Phelan (WP) space-filling honeycombs [36].

Actually, Aluminum foams are also available on the market for several manufactures.

4.2 The experimental apparatus for SEY studies

The SEY is defined as the ratio of the number of electrons leaving the sample surface ($I_{out}(E)$) to the number of incident electrons ($I_p(E)$) per unit area. In particular, $I_{out}(E)$ can be calculated as the difference between the current impinging on the sample $I_p(E)$ and the current flowing from the sample $I_s(E)$ (see Eq. 4.1).

$$\delta(E) = \frac{I_{out}(E)}{I_p(E)} = \frac{1 - I_s(E)}{I_p(E)} \tag{4.1}$$

It is possible to measure the SEY of a technical surface using two different experimental schemes [19]:

- $I_p(E)$ and $I_s(E)$ are separately gauged. In this case, the impinging electron current is measured by a Faraday Cup, in Fig. 4.2 a);
- $I_{out}(E)$ and $I_s(E)$ are simultaneously measured. The electrons are collected either from a cage around the gun placed in front of the sample (see Fig. 4.2 b)) or using an hemispherical collector all around the system.

All methods produce very similar results.

The experiments shown in this chapter were performed at the Material Science INFN-LNF laboratory of Frascati (Roma).
The apparatus operates in a Ultra-High Vacuum (UHV) μ-metal chamber with a pressure below 10^{-10} mbar. The residual magnetic field at the sample position is less than 5 mG. In this way, the measure of the currents at low energy is not affect by the magnetic field.
In our set-up the SEY measurement were performed by two subsequent operation: a) collect the sample electron current $I_s(E)$ as a function of the intensity and

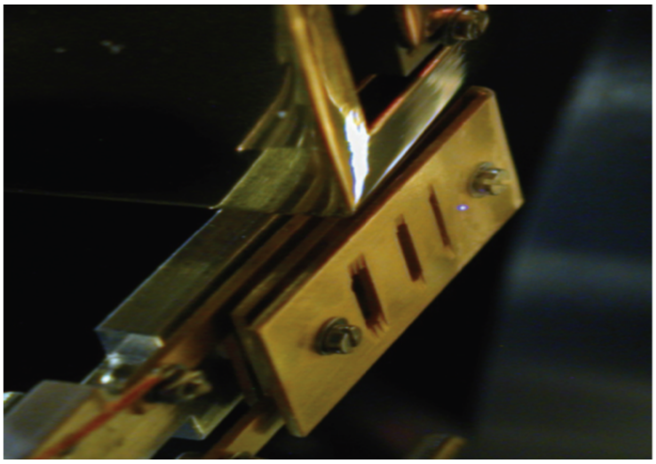

(a) Faraday cup used to measure $I_p(E)$ in different experiment. Each wide slot (1,2,3 mm) can be driver into the beam to measure the beam profile. The blu spot on the right side is the electron beam (500 eV) hitting a fluorescent powder previously deposed on the external part of the Faraday cup

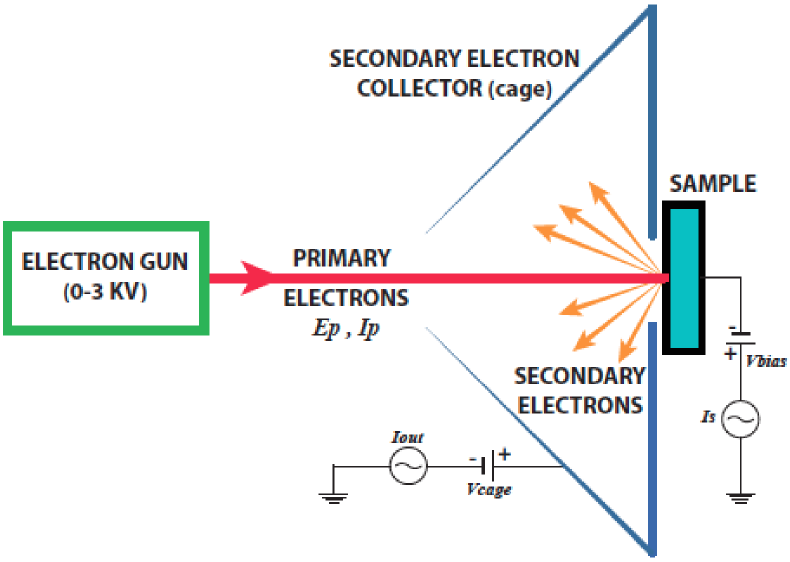

(b) SEY experimental apparatus in use at CERN to measure $I_{out}(E)$ and $I_s(E)$. Readapted from N.Hilleret

FIGURE 4.2: Different SEY experimental apparatus

energy of the landing primary electron beam E_p; b) collect the e-gun emitted current $I_p(E_g)$ by using an "ad hoc" designed Faraday cup. Stability of SEY can be guaranteed if a series of repeated measurements give, within few percent, the same $I_p(E)$.
To finally calculate $\delta(E)$ it was necessary to scale the energy (E_g) at which $I_p(E)$ was emitted by the electron gun and measured with the Farady cup, to the final landing primary energy (E_p) by considering the applied retarding voltage V_b [34].

Other experimental studies were carried out at CERN to validate and complete the data and to obtain the complementary information required for a safe use in UHV and in accelerator technology.

4.3 SEY measurements: preliminary results

Cu foam samples are cut in different sizes from a 6 mm thick slabs of different porosity (4, 8, 16 pores/cm) supplied from Goodfellow Inc.
Experimentally, dealing with such non uniform and nearly transparent material, it is intrinsically quite difficult and several aspects, new to those materials, have to be taken into account in order to produce significant SEY data.
The first obvious difficulty in measuring SEY on foams is due to the size of the electron beam used in SEY experiments since it is extremely small in respect to the macroscopic size of the foam and the density of the pores. Another important aspect is the shape and orientation of the Cu mesh which can strongly influence the SEY measurements. In fact, the beam hitting the sample can be driven into the foam or bounce back, according to where it impacts.
To tackle this difficulty a series of repeated SEY spectra were collected moving the electron beam in small steps in a (2x3 mm^2) area within the sample. In this way, we are able to mediate the inhomogeneity surface collecting many spectra from nearly overlapping irradiation points.
The result of this method is shown in Fig. 4.3, in which we report all the SEY spectra collected on a Cu foam of 8 pores/cm.

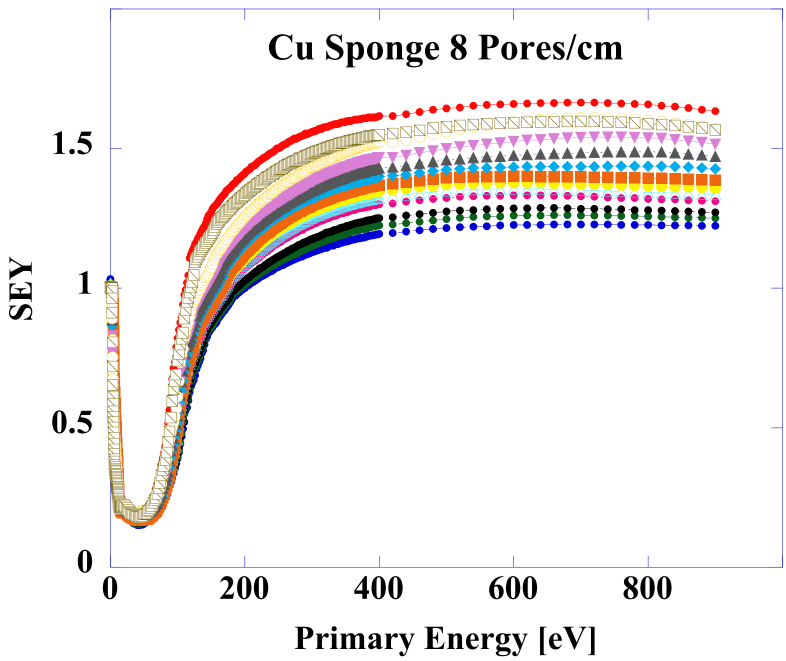

FIGURE 4.3: SEY spectra obtained by moving the electron beam in a small steps in a (2x3 mm^2) area within a 8 pores/cm Cu foam mounted in a 6x6x6 Cu cage.

The second problem, which is intrinsic to the foams and to their high transparency is that the results depend on sample size and on the way such samples are mounted on the sample holder.

In this work, we show data from embedded Cu foam with different porosity in a 6x6x6 mm^3 cage.The results shown are than valid only for this geometry which was chosen being representative of the SEY of a such Cu foams lying on a copper plate and with no free sides.

Average SEY from different porosity foams embedded in a Cu cage are reported in fig. 4.4 together with the error bars of about $\pm 20\%$. This value was estimated from the analysis of data shown in Fig. 4.3.

On a fully embedded foam we can observe:

- a significant overall decrease of the SEY in comparison with the SEY of a Cu "as received" surface representative of the LHC beam screen also plotted in fig. 4.4 and taken from the literature [19];

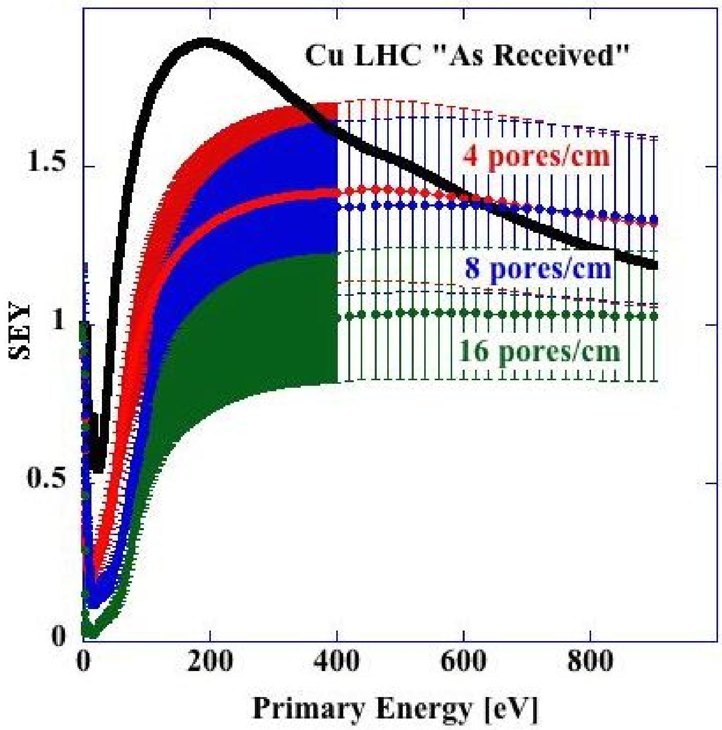

FIGURE 4.4: SEY spectra obtained for differ Cu Foam. The black curve represents the SEY measured on a flat Cu onto Stainless steel substrate as in the LHC beam screen.

- a smaller SEY for higher porous density foam, with δ_{max} going from 2 (for LHC Cu) to 1.5 - 1.4 (for the 4 and 8 pores/cm foams) and less than 1 (for the 16 pores/cm foam).

On the other hands, if the foam were freestanding one would expect that the lower density pores foams, having bigger holes and less material interacting with the beam, would show a lower SEY than higher density pores.
The presence of the cage in the experiment justifies the observed opposite trend of the SEY versus the porosity of the sample. Increasing the transparency of the foam, more electrons can reach the Cu holder, which has a δ_{max} equal to 2. In this way, the SEY measured is greater.

Looking at Fig. 4.4, another interesting aspect which can be observed is the gradual increase of the region of very low SEY, at low energy, as a function of the porosity. As itis shown, for supported foams the low energy electrons tend to be absorbed by the pores. The reasons of this behavior will be discuss in other works.

In the end, our preliminary results obtained suggest that, when compatible with geometrical constrains, Cu foams can be utilized as EC moderator in future particle accelerators.

Chapter 5

Summary and conclusions

Electron Cloud (EC) effects represent a serious limitation for particle accelerators operating with intense beams of positively charged particles. This thesis presents simulation and experimental studies on EC effects carried out in collaboration with the European Organization for Nuclear Research (CERN) in Geneva and with the INFN-LNF laboratories in Frascati.

The modeling and simulation work has focused mainly on the CERN Proton Synchrotron (PS). The PS has resumed operation after the Long Shutdown 1 (LS1, 2013-2014) with newly installed instrumentation for the direct monitoring of the EC inside one of the main magnets. This device, which is able to measure the electron flux to the chamber walls, will allow to investigate the EC formation in presence of strong magnetic fields. Numerical simulations with the newly developed PyECLOUD code have been performed in order to quantify the expected signal at the detector under different beam conditions.

Before starting the implementation of the new PS EC detector in PyECLOUD, we decided to simulate the case of the strip monitor installed in the Super Proton Synchrotron (SPS) since for this detector data obtained with the older ECLOUD code were already available and the results of the new PyECLOUD simulations could be directly benchmarked against previous ones. The SPS EC strip monitor is installed inside one of the dipole magnets of the ring. Its liner features several symmetric and periodic rows of holes drilled directly in the side of the chamber in front of a detector made of 48 copper strips. For this detector, the results of the simulations were found in good agreement with the old data confirming that the implementation of the EC detector in PyECLOUD is correct. Moreover this study could investigate in detail interesting features of the EC buildup inside this kind of device, i.e. the dependence electron distribution on the applied magnetic field and the impact of the presence of the holes on the EC multipacting threshold.

Later on we moved to the implementation of the PS EC detector. Similarly to the case of the SPS detector, the holes were modeled as regions of the wall with SEY equal to zero. The count of electrons impinging against these regions provides the electron signal that is measured by the collector.

The presence of the strong and non-uniform magnetic field of the PS combined function magnet makes these simulations quite challenging from the numerical point of view. Therefore several checks were performed before starting the actual simulation study. It was found that the semi-analytic algorithm which is usually used in PyECLOUD simulations, especially for dipole magnets, introduces an unphysical drift of the electron distribution in the horizontal plane, with strong artifacts on the simulated detected current. This effect disappears when performing the simulations with a Boris tracker, which allows to correctly evaluate the electron signal through the holes.

Convergence scans with respect to the simulation time steps were performed in order to find a good balance between simulation accuracy and computation time. A good convergence was achieved for a simulation time step of 25 ps and 10 Boris substeps per main simulation step.

The sensitivity of the simulations to the initial distributions of primary electrons in the chamber was also investigated. With this respect it was found that, in order to minimize the noise on the electron profile, it is necessary to use a large number of macroparticles and to initialize them uniformly inside the cross section of the beam pipe.

The identified simulation setup was then used to investigate the behavior of the EC detector under different beam conditions, in terms of bunch length and bunch population. The results show that the multipacting threshold decreases when the bunch length decreases and when the bunch intensity increases.

Due to design constraints, the detector is slightly displaced with respect to the vertical axis of the chamber cross section. For this reason the dependence of the detected signal on the radial position of the beam was also investigated. By scanning the beam position by ∓ 3 cm around the nominal orbit, we found that the electron flux through the holes is strongly affected by the beam displacement. In particular, it becomes acceptable only when the beam gets closer to the region of the detector, i.e. more than 1 cm far from the center of the chamber.

The experimental activity, carried out at the INFN-LNF laboratories in Frascati, was focused on the characterization of Cu foams as a mean for mitigating EC effects. Preliminary data, representative of a Cu foams embedded in a Cu cage, show a significant SEY reduction and interesting peculiarities of such modified structures. During the experimental activity, several issues have been identified mainly related to the high inhomogeneous and partly transparent structure. In order to better qualify the Cu foams as a mature technology to use in the accelerator system, more data with different experimental geometries and measuring setups, are required. Our preliminary results suggest a potentially interesting use of the Cu foams as a EC moderator in future particle accelerators.

Acknowledgements

Non é facile ringraziare, in poche righe, tutte le persone che hanno contribuito alla nascita e allo sviluppo di questa tesi di laurea.
Innanzitutto vorrei ringraziare la Prof.Stefania Petracca per avermi offerto la possibilitá di lavorare ad un tema cosí interessante ed ambizioso, in collaborazione sia con l'INFN-LNF di Frascati che con il CERN di Ginevra, ma sopratutto per avermi guidato in questa esperienza spronandomi continuamente a dare il meglio. Sicuramente tutto ció mi ha aiutata a crescere sia professionalmente che umanamente.
Un grazie speciale va a Giovanni per aver creduto in me dandomi la possibilitá di intraprendere questa fantastica avventura al CERN (chí mi conosce sá quanto ci tenessi!). I suoi consigli sono stati determinati per la riuscita di questo lavoro..... Grazie per la tua disponibilitá!
Grazie anche a Roberto che mi ha guidato nel mio percorso all INFN, sicuramente se sono arrivata qui piú pronta é anche grazie ai tuoi insegnamenti.
Rosanna...a te va un GRAZIE! Grazie per la tua disponibilitá, per la tua pazienza infinita nei miei confronti, per avermi insegnato tanto ...anzi tutto!
Sei stata sicuramente una figura preziosissima.

Ma nn avrei potuto fare nulla di tutto ció senza Gianni. Bhé... che dire!!! Senza i suoi pazienti insegnamenti, le sue risposte sempre pronte, il suo incoraggiamento ...sicuramente questa tesi non avrebbe prodotto alcun risultato. A lui sono in particolar modo profondamente riconoscente.
E poi vorrei ringraziare anche molti membri della mia sezione HSC, perché ognuno a proprio modo e spesso inconsapevolmente mi ha insegnato qualcosa.

Poi ci sono gli amici, coloro che mi hanno aiutata nei momenti difficili e gioito, con e per me, quando raggiungevo un traguardo. La mia gratitudine vá a Claudia e Letizia, per avermi guidato in questa avventura senza mai farmi sentire sola. E poi ci sono Giorgia, Eleonora, Daniele, Georges, Vincenzo, Stefano.....quando si sta in gruppo si sá, tutto diventa meno faticoso!!!

Grazie a chi ha vissuto (letteralmente) con me in questo periodo:Donato ed Alessandro. Tra alti e bassi, e nonostante tutto, un ottimo trio.
E poi ci sono loro Mario e Andrea (lo zio),é sopratutto grazie a voi che questa é e rimarrá, una delle esperienze piú belle che abbia mai intrapreso.
A buon intenditore, poche parole!

Quando cresci ed inizi a fare nuove esperienze tante persone entrano a far parte della tua vita, quasi senza accorgertene. Qualcuna con il tempo la perdi, qualcun' altra la trovi...e poi c' é chi, nonostante il tempo e la lontananza, é sempre lí: le tue amiche. Se mi hanno sopportato in tutti questi anni, sono sicura che lo faranno ancora. Grazie a voi, perché se sono qui é anche e sopratutto merito vostro!

Emanuela, tu! La storia di come e quando ci siamo conosciute ormai la conosce chiunque abbia letto i ringraziamenti della tesi precedente.....e questo la dice molto lunga sul nostro rapporto! Eri con me il giorno in cui mi é arrivata quell' email cosí tanto attesa....come dimenticarlo! Sapevi cosa significasse per me partire ed arrivare fin qui, forse proprio per questo mi hai sempre incitata a stringere i denti e a non mollare. Per la prima volta, abbiamo intrapreso percorsi diversi ma nonostante tutto siamo sempre rimaste vicine, solidali l'una con l'altra ...forse ancora piú di prima. Forse non te l'ho mai detto....grazie!

Dulcis in fundo, un grazie speciale alla mia famiglia.
Ai miei genitori che sono stati sempre al mio fianco sopratutto in quest'anno pieno di novitá e cambiamenti ... non solo per me ma anche per loro. Questo lavoro é anche vostro.
La scoperta degli ultimi anni, mio fratello. Sicuramente la persona che piú di tutte, anche se tacitamente, crede in me. La cosa piú bella del nostro rapporto é che si rafforza di anno in anno.
Mio caro, aspetto con ansia i tuoi di ringraziamenti..... ed ho detto tutto!

Bibliography

[1] S. Petracca and A. Stabile. Open cell conducting foams for high synchrotron radiation beam liners. *Phys. Rev. ST Accel. Beams 17, 083503.*

[2] W. Fischer, M. Blaskiewicz, J.M. Brennan, H. Huang, H.C. Hseuh, V. Ptitsyn, T. Roser, P. Thieberger, D. Trbojevic, J. Wei, S. Y. Zhang, and U. Iriso. Electron cloud observations and cures in the relativistic heavy ion collider. *Physical Review Special Topics-Accelerators and Beams*, 11(4):041002, 2008.

[3] H. Fukuma. Electron Cloud Observations and Predictions at KEKB, PEP-II and SuperB Factories. *Proceedings of ECLOUD12: Joint INFN-CERN-EuCARD-AccNet Workshop on Electron-Cloud Effects, La Biodola, Isola d'Elba, Italy*, 2012.

[4] M. Zobov, D. Alesini, A. Drago, A. Gallo, S. Guiducci, C. Milardi, A. Stella, S. De Santis, T. Demma, and P. Raimondi. Operating experience with electron cloud clearing electrodes at DAFNE. *Proceedings of ECLOUD12: Joint INFN-CERN-EuCARD-AccNet Workshop on Electron-Cloud Effects, La Biodola, Isola d'Elba, Italy*, 2012.

[5] G. Iadarola, G. Arduini, V. Baglin, H. Bartosik, J.E. Esteban Müller, G. Rumolo, E. Shaposhnikova, L. Tavian, F. Zimmermann, O. Domínguez, and G.H.I. Maury Cuna. Electron Cloud and Scrubbing Studies for the LHC. *Proceedings of the IPAC13 International Particle Accelerator Conference, Shanghai, China*, 2013.

[6] J.R.M. Vaughan. Multipactor. *Electron Devices, IEEE Transactions on*, 35 (7):1172–1180, Jul 1988. ISSN 0018-9383. doi: 10.1109/16.3387.

[7] R. A. Kishek, Y. Y. Lau, L. K. Ang, A. Valfells, and R. M. Gilgenbach. Multipactor discharge on metals and dielectrics: Historical review and recent theories. *Physics of Plasmas (1994-present)*, 5(5):2120–2126, 1998. doi: http://dx.doi.org/10.1063/1.872883. URL `http://scitation.aip.org/content/aip/journal/pop/5/5/10.1063/1.872883`.

[8] A. Woode and J. Petit. Investigations into multipactor breakdown in satellite microwave payloads. *ESA Journal*, 14:467–478, 1990.

[9] G. Rumolo, F. Ruggiero, and F. Zimmermann. Simulation of the electron-cloud build up and its consequences on heat load, beam stability, and diagnostics. *Phys. Rev. ST Accel. Beams*, 4:012801, Jan 2001. doi: 10.1103/PhysRevSTAB.4.012801. URL `http://link.aps.org/doi/10.1103/PhysRevSTAB.4.012801`.

[10] G. Peach. Ionization of atoms and positive ions by electron and proton impact. *Journal of Physics B: Atomic and Molecular Physics*, 4(12):1670, 1971. URL `http://stacks.iop.org/0022-3700/4/i=12/a=015`.

[11] G. Iadarola. *Electron cloud studies for CERN particle accelerators and simulation code development*.

[12] M. E. Rudd, Y. K. Kim, D. H. Madison, and J. W. Gallagher. Electron production in proton collisions: total cross sections. *Rev. Mod. Phys.*, 57: 965–994, Oct 1985. doi: 10.1103/RevModPhys.57.965. URL `http://link.aps.org/doi/10.1103/RevModPhys.57.965`.

[13] J. D. Jackson. *Classical electrodynamics*. Wiley, New York, NY, 3rd ed. edition, 1999. ISBN 9780471309321. URL `http://cdsweb.cern.ch/record/490457`.

[14] A. Hofmann. *The Physics of Synchrotron Radiation*. Cambridge Monographs on Particle Physics, Nuclear Physics and Cosmology. Cambridge University Press, 2004. ISBN 9781139451109. URL `http://books.google.fr/books?id=oHs9HUMncQcC`.

[15] E. Willett. *The Basics of Quantum Physics: Understanding the Photoelectric Effect and Line Spectra*. The Library of Physics. Rosen Publishing Group, 2004. ISBN 9781404203341. URL `http://books.google.it/books?id=P4ADT5eJ8roC`.

[16] R. Cimino, I. R. Collins, M. A. Furman, M. Pivi, F. Ruggiero, G. Rumolo, and F. Zimmermann. Can Low-Energy Electrons Affect High-Energy Physics Accelerators? *Phys. Rev. Lett.*, 93:014801, Jun 2004. doi: 10.1103/PhysRevLett.93.014801. URL `http://link.aps.org/doi/10.1103/PhysRevLett.93.014801`.

[17] A.W. Chao. *Physics of Collective Beam Instabilities in High Energy Accelerators*. Wiley Series in Beam Physics and Accelerator Technology. Wiley, 1993. ISBN 9780471551843. URL `http://books.google.fr/books?id=MjRoQgAACAAJ`.

[18] L. Tavian. Performance Limitations of the LHC Cryogenics: 2012 Review and 2015 Outlook. *Proceedings of the Evian 2012 LHC Beam Operation Workshop, Evian, France*, 2012.

[19] R. Cimino and T. Demma. Electron cloud in accelerators. *International Journal of Modern Physics A*, 2014.

[20] C. Yin Vallgren, G. Arduini, J. Bauche, S. Calatroni, P. Chiggiato, K. Cornelis, P. Costa Pinto, E. Métral, G. Rumolo, E. Shaposhnikova, M. Taborelli, and G. Vandoni. Amorphus carbon coatings for mitigation of electron cloud in the CERN SPS. *Proceedings of IPAC10, Kyoto, Japan*, 2010.

[21] G. Iadarola and G. Rumolo. PyECLOUD and Build Up Simulations at CERN. *Proceedings of ECLOUD12: Joint INFN-CERN-EuCARD-AccNet Workshop on Electron-Cloud Effects, La Biodola, Isola d'Elba, Italy*, 2012.

[22] S. Gilardoni and D. Manglunki. Fifty years of the CERN Proton Synchrotron, Volume I. *CERN-2011-004*.

[23] S. Garoby, H. Hancock, and J.L. Vallet. Demonstration of bunch triple splitting in the CERN PS. *Proceedings of EPAC 2000*.

[24] R. Cappi, M. Giovannozzi, E. Métral, G. Métral, G. Rumolo, and F. Zimmermann. Electron cloud buildup and related instability in the cern proton synchrotron. *Phys. Rev. ST Accel. Beams*, 5:094401, Sep 2002. doi: 10.1103/PhysRevSTAB.5.094401. URL `http://link.aps.org/doi/10.1103/PhysRevSTAB.5.094401`.

[25] R. Steerenberg, G. Arduini, E. Benedetto, A. Blas, W. Höfle, E. Métral, M. Morvillo, C. Rossi, and C. Rumolo. Nominal LHC Beam Instability Observations in the CERN Proton Synchrotron. *Proceedings of the 22nd Particle Accelerator Conference, Albuquerque, NM, USA*, 2007.

[26] E. Mahner, T. Kroyer, and F. Caspers. Electron cloud detection and characterization in the cern proton synchrotron. *Phys. Rev. ST Accel. Beams*, 11:094401, Sep 2008. doi: 10.1103/PhysRevSTAB.11.094401. URL `http://link.aps.org/doi/10.1103/PhysRevSTAB.11.094401`.

[27] G. Iadarola, H. Damerau, S. Gilardoni, G. Rumolo, G. Sterbini, C. Yin Vallgren, M. Pivi, and S. Rioja-Fuentelsaz. Electron Cloud Studies for the Upgrade of the CERN PS. *Proceedings of the IPAC13 International Particle Accelerator Conference, Shanghai, China*, 2013.

[28] C. Yin Vallgren, P. Chiggiato, and S. Gilardoni. Development of the new electron cloud detectors in the ps. URL `https://indico.cern.ch/event/323569/contribution/1/material/slides/0.pdf`.

[29] C. Yin Vallgren, G. Arduini, J. Bauche, S. Calatroni, P. Chiggiato, K. Cornelis, P. Costa Pinto, B. Henrist, E. Métral, H. Neupert, et al. Amorphous carbon coatings for the mitigation of electron cloud in the cern super proton synchrotron. *Physical Review Special Topics-Accelerators and Beams*, 14(7):071001, 2011.

[30] G. Iadarola and G. Rumolo. Improving pyecloud accuracy for quadrupole simulations: ongoing work. URL `https://indico.cern.ch/event/310641/contribution/3/material/slides/3.pdf`.

[31] A.A. Krasnov. Molecular pumping properties of the lhc arc beam pipe and effective secondary electron emission from cu surface with artificial roughness. *Vacuum, Vol 73, p. 195–199.*

[32] G. Stupakov and M. Pivi. Suppression of the effective secondary emission yield for a grooved metal surface. *Proceedings of ECLOUD2004: 31st ICFA Advanced Beam Dynamics Workshop on Electron-Cloud Effects,Napa, CA.*

[33] M.T.F et al. Pivi. Sharp reduction of the secondary electron emission yield from grooved surfaces. *J.Appl.Phys. 104.*

[34] R. Cimino, A. Romano, S. Petracca, A. Stabile, M.R. Masullo, G. O'Connor, S. abd Bregliozzi, and V. Baglin. Search for new e-cloud mitigator materials for high intensity particle accelerators. *Proceedings of IPAC 2014.*

[35] J. Banhart and N.A. Fleck. Cellular metals and metal foaming technology. 2003.

[36] D. Weaire and P. Phelan. *A counterexample to Kelvin's conjecture on minimal surfaces.* Phil. Mag. Lett. vol. 69, 107-110, 1994.